74 pages

Perturbations of the Richardson Number Field by Gravity Waves

M. G. Wurtele, Principal Investigator

R. D. Sharman, Co-Investigator

Department of Atmospheric Sciences, UCLA, Los Angeles, CA 90024

Final Technical Report

under

NASA NSG 4024

"Models for numerical simulation of gravity

waves and CAT formation"

Period of Report: May 1, 1979 to December 31, 1984

Date of Report: 1 July 1985

1. Introduction

Many gravity wave studies have been motivated entirely or in part to determine the perturbation introduced by the wave into the Richardson number field (e.g., Keller et al., 1983; Wurtele and Sharman, 1983; Thorpe, 1981; Fritts, 1979; Gossard and Hooke, 1975; Scorer, 1969). However, there have been few attempts at a systematic investigation of this problem, and since the Richardson number is a rather complex combination of the basic variables, it is difficult, even in the linear case, to form a conception of the Richardson number field, given the fields of the basic variables.

Gossard and Hooke (1975, Section 36) derive the relevant formulas, and present a single calculation of a three layer model; but this model has infinite initial Richardson number and consequently is not well suited to compute Richardson number changes induced by gravity waves.

In non-Boussinesq models, as is well known (Lamb, 1932), perturbation quantities increase in magnitude exponentially with height; and this effect has occasioned interest as a mechanism in the middle atmosphere for producing negative static stability (Hodges, 1967; Lindzen, 1981). Here we are concerned with the Boussinesq dynamics of the resonance lee wave, which dies out exponentially above its level of trapping. Since the trapping mechanism is wind shear, the upstream Richardson number is necessarily finite; however, the plane wave solution is not applicable.

We propose here (1) to derive analytic solutions for an appropriate linear model with finite initial Richardson number, so that we may study the perturbed Richardson number field as a function of the mean flow parameters; (2) to execute numerical time-dependent simulations to compare with the analytic results; and (3) to obtain some useful qualitative non-linear formulations.

2. Linear analysis

If ψ' is the perturbation stream function, w' the vertical velocity, u_0 and u' the mean and perturbation horizontal velocities, respectively, δ' the vertical displacement, and ζ' the vorticity, then we have, under steady state conditions,

$$\zeta' = \nabla^2 \psi'$$

$$w' = \frac{\partial \psi'}{\partial x} = u_0(z) \frac{\partial \delta'}{\partial x} \tag{1}$$

where subscript zero indicates mean-flow quantities.

The Boussinesq bouyancy, $\sigma' = g\rho'/\rho_{00}$, where ρ' is the perturbation density, and ρ_{00} a reference density, is related to these quantities by

$$\sigma' = N_0^2 \delta' = N_0^2 \psi'/u_0$$

where N_0 is the Boussinesq Brunt frequency, $N_0^2 = -g d\rho_0/\rho_{00} dz$, for the mean density.

We denote the perturbation stream function wave amplitude by

$$\psi' = \hat{\psi}(z) \sin k x \tag{2}$$

where k is the horizontal wavenumber of the disturbance, and similarly for other variables. The familiar vertical structure equation for the stream function is (Scorer, 1949):

$$\frac{d^2\hat{\psi}}{dz^2} + (\ell^2 - k^2)\hat{\psi} = 0, \tag{3a}$$

where

$$\ell^2 = \frac{N_o^2}{u_o^2} - \frac{1}{u_o} \frac{d^2 u_o}{dz^2} \qquad (3b)$$

The Richardson number for the perturbed flow may be written as

$$Ri = \frac{N_o^2 - d\sigma'/dz}{\left(\frac{du_o}{dz} + \frac{du'}{dz}\right)^2} = Ri_o \frac{1 - d\sigma'/N_o^2 dz}{[1 + (du'/dz)(du_o/dz)^{-1}]^2} \qquad (4)$$

where $Ri_o = N_o^2/(du_o/dz)^2$ is the Richardson number of the mean flow. In terms of the vertical displacement $\hat{\delta}$, (4) becomes, using (1), (2) and (3):

$$Ri/Ri_o = \frac{1 - [(d\hat{\delta}/dz) + (dN_o^2/N_o^2 dz)\hat{\delta}] \sin kx}{[1 + \ell^2 u_o (du_o/dz)^{-1} \hat{\delta} \sin kx]^2} \qquad (4a)$$

A similar expression in terms of $\hat{\psi}$ is

$$Ri/Ri_o = \frac{1 - [(\hat{\psi}/u_o) + (\hat{\psi} dN_o^2/N_o^2 u_o dz) - (du_o/dz)^2 \hat{\psi}] \sin kx}{[1 + \ell^2 (du_o/dz)^{-1} \hat{\psi} \sin kx]} \qquad (4b)$$

Equation (4b) reduces to equation (36-12) of Gossard and Hooke (1975) in the case N_o^2 = constant.

We now require a simple solution for a stable sheared flow permitting trapped waves, in which we may exhibit the pattern of the Richardson number field along side of the fields of ψ,' w, u', and σ'. One candidate model is that of Palm and Foldvik (1960) for a flow in which the mean velocity is exponentially increasing with height. In this model, however, the mean Richardson number is therefore also exponentially varying, with the result

that it is difficult to interpret the perturbed Richardson number field. Interpretation is greatly facilitated if the basic Ri-field is uniform with height.

An analytic solution for such a model has been presented by Wurtele (1953). This model assumes constant mean wind shear and stability, and therefore a constant Richardson number; however, it includes certain non-Boussinesq terms, for reasons to become apparent below. It has been known since the beginning of lee-wave theory (e.g., Scorer, 1949) that if both density gradients and potential termperature gradients are taken into account, and if

$$\rho_0(z) = \rho_{00}\exp(-\beta z) \qquad\qquad \beta = \text{const.}$$

and

$$\theta_0(z) = \theta_{00}\exp(N_0^2 z/g) \qquad\qquad N_0^2 = \text{const.}$$

then the density-weighted variable

$$\hat{\phi} = \left(\frac{\rho_0}{\rho_{00}}\right)^{-\frac{1}{2}} \hat{\psi}$$

satisfies the equation

$$\frac{d^2\hat{\phi}}{dz^2} + \left(\frac{N_0^2}{u_0^2} - \frac{1}{u_0}\frac{d^2 u_0}{dz^2} - k^2 - \frac{\beta^2}{4}\right)\hat{\phi} = 0 \ . \tag{6}$$

Some now-familar approximations are involed in deriving this equation (Scorer, 1949). The introduction of a constant mean wind shear into the model,

$$u_0 = U(1 + z/L) \qquad\qquad U, L \text{ constant}$$

thus provides a constant mean Richardson number

$$Ri_0 = N_0^2 L^2 / U^2$$

against which one may study the perturbations arising out of the gravity-wave disturbance. If variables are rendered dimensionless by the scalings

$$Z = 1 + z/L, \quad \phi^* = \phi/UL, \quad k_* = kL, \quad \beta_* = \beta L$$

the vertical structure equation (6) becomes

$$\frac{d^2\phi^*}{dZ^2} + \ell_*^2 \phi^* = 0 \tag{7}$$

where

$$\ell_*^2(Z) = \frac{Ri_0}{Z^2} - \kappa^2 ,$$

and

$$\kappa^2 = k_*^2 + \beta_*^2/4 ,$$

and equations (4a,b) for the Richardson number become

$$Ri/Ri_0 = \frac{1 - \frac{d\delta_*}{dZ} \sin kx}{\left[1 + \ell_*^2 Z \delta_* \sin kx\right]^2} \tag{8a}$$

where

$$\delta_* = \left(\frac{\rho_0}{\rho_{\infty}}\right)^{\frac{1}{2}} \frac{\hat{\delta}}{L}$$

and

$$Ri/Ri_0 = \frac{1 - \left[\frac{1}{Z}\frac{d\phi_*}{dZ} - \frac{\phi_*}{Z^2}\right] \sin kx}{\left[1 + \ell_*^2 \phi_* \sin kx\right]^2} \tag{8b}$$

The most convenient representation of the Richardson number field is the percentual change from the initial or mean field Ri,

$$\frac{\Delta Ri}{Ri_0} = \frac{Ri}{Ri_0} - 1 \; .$$

From equations (7), we see that this quantity must be in phase with the fields of ψ' and u'_s and 90 degrees out of phase with w. However, Ri is not linearly related to these fields, owing to the modification by the denominator. To see the effect of this shear term, consider the levels at which displacements have a maximum or minimum, i.e., $\frac{d\,\delta_*}{dZ} = 0$. Then expanding the denominator by the approximation

$$(1 + \epsilon)^{-2} = 1 - 2\epsilon + \epsilon^2 \; ,$$

we have from (8a)

$$\frac{\Delta Ri}{Ri_0} = -2\,\ell^2\,\delta_* \sin kx + 3(\,\ell^2\,\delta_* \sin kx\,)^2 \; .$$

Thus the percentual change in the Richardson number will be larger in magnitude when it is positive than when it is negative. We shall see in the simulations that this effect is important even for very small perturbations.

The term $\frac{d\,\delta_*}{dZ}$ in the numerator of (8a) is the linearized representation of the vertical stretching or shrinking (and hence the modification of the static stability) of an infinitesimal column of air when vertically displaced. The term $\ell^2\delta_*$ in the denominator obviously arises from the structural equation (7), which gives the perturbation shear in terms of stream function or vertical velocity. The factor Ri_0 in this term suggest that it will dominate over the modification of N^2 in the numerator for the normal range of atmospheric

Richardson numbers. It also follows that the effect of the shear decreases with elevation and wave number. As will be shown, this hypothesis is borne out quantitatively in both analytic solutions and simulations.

The solution to equation (6) regular as $Z \to \infty$ may be written simply as (Wurtele, 1953)

$$\phi_* = \phi_{00} Z^{\frac{1}{2}} K_{i\mu}(\kappa Z) \qquad\qquad 1 \leq Z \leq \infty \qquad (9)$$

where $\mu^2 = Ri_0 - 1/4$, and $K_{i\mu}$ is a modified Bessel function of imaginary order. This function is oscillatory in its argument for small argument and falls off exponentially for large argument. It is discussed and diagrammed in Appendix A.

Thus, depending on the relative magnitudes of μ and κ, the solution (9) permits a finite number, possibly zero, of gravity wave free modes, forced at $z = 0$ ($Z = 1$) and trapped at elevations inversely proportional to their wave lengths, and dying out exponentially above their level of trapping. The free modes (at $z = 0$) are given by

$$K_{i\mu}(\kappa) = 0 \ , \qquad\qquad\qquad (10)$$

that is, solutions satisfying a homogenous condition at the boundary. We shall be concerned only with conditions for which one or two wave solutions, or free modes, exist. These are determined by evaluation of the Bessel function by computer, as outlined in Appendix A.

The effect of the non-Boussinesq term β now becomes evident. The function $K_{i\mu}(\kappa)$ is singular as $\kappa \rightarrow 0$, becoming infinitely oscillatory (see Appendix A). In this model, regardless of how small k is, κ will be limited below by $\beta/2$. Thus the non-Boussinesq effect is to filter out all waves longer than the gravity wave asssociated with the mean density gradient. Another instance in which this effect permits a mathematically consistent solution occurs in the internal wave study by Mowbray and Rarity (1967). Our simulation model is entirely Boussinesq in its formulation; but in a simulation, of course, the longer waves ($k \rightarrow 0$) are eliminated simply by virtue of the limited horizontal and vertical extent of the computational grid. Since the wave length associated with the wave number $\beta/2$ is of the order of 100 km and greater, this constitutes no limitation to the present study.

The wave solution is related to its kinematic forcing at the boundary by a technique that is too familiar to warrant repetition here (Wurtele, 1953; Palm and Foldvik, 1960; Queney, 1960). We assume a surface of the form known as the "Witch of Agnesi"

$$h(x) = \frac{H\,a^2}{a^2 + x^2}$$

which has the convenient Fourier transform $\hat{h}(k) = H\,a\,\exp(-a|k|)$. The integral expression for the perturbation stream function is then

$$\psi'(x,z) = \frac{U\,H\,a}{2} \int_{-\infty}^{\infty} e^{ikx - ak} \frac{K_{i\mu}(\kappa z)}{K_{i\mu}(\kappa)} \, dk \tag{11}$$

We follow the procedure referred to above, using the method of residues, and taking the principal value of the integral when poles exist in such a way as to cancel the upstream wave.

The result is a wave solution, provided (10) is satisfied for some $k = k_1$, that has the form

$$\psi'(x,z) = -2\pi a e^{-k_1 a} \frac{UH}{L} \frac{K_{i\mu}(\kappa_1 z)}{K'_{i\mu}(\kappa_1)} \sin kx \qquad (12)$$

where $K'_{i\mu}$ is the derivative of $K_{i\mu}$ with respect to its argument.

If other roots of (10) exist, these are of the same form and the solutions are additive. There is of course, in addition, a forced monotonic part of the solution that dies out exponentially both upstream and downstream, and does not concern us here.

In the linear analytic computations we have calculated ψ' from (12), other variables from the linear relationships, and the Richardson number field from (8).

The comparison numerical simulations are computed not for purposes of verification, but in order to identify limits on the assumption of linearity. As will appear below, this is not entirely a straightforward matter. The simulations are computed with the Boussinesq code described by Sharman and Wurtele (1983) and more fully by Sharman (1981). In every case, the computations are performed with a linear surface boundary condition, but with all non-linear terms present in the dynamic equations. The comparisons with the analytic computations thus isolate the departures from linearity due to the dynamics from those inherent in the calculation of the Richardson number itself.

3. Results of the analysis and simulations.

Linearity in lee-wave problems is conventionally assessed by the parameter NH/U and we accept this criterion for the moment. For a sensitivity study of this parameter under the conditions N = const, U = const, see Miles (1965). Results will be presented for a variety of cases which are defined by Ri_o and NH/U. (See Table I for summary of cases and figures.)

Figure 1 (a,b,c,d) presents the analytically derived perturbation fields for the conditions of Case I described in the legend. Note that as mentioned above in this and all computations herein, the Brunt frequency and wind shear are uniform, so that the basic Richardson number is also uniform with height.

The conditions assumed for Case I specify $Ri_0 = 8$ and NH/U = 0.1, a highly linear problem, as will be seen below. Figures 1a and 1b show, respectively, the perturbation stream function and the vertical velocity. Figure 1c contains contours of total horizontal velocity, and the smallness of the perturbation relative to the mean flow is evident. In the areas near the surface where the total horizontal speed is reduced (i.e., where the contours of Figure 1c are lifted), the shear is increased, and the Richardson number is decreased. Conversely, where the total horizontal speed is increased, the shear is decreased, and the Richardson number is increased. This qualitative assessment is borne out in Figure 1d, which presents contours of the Richardson number. Quantitatively, however, we see, consistent with the analysis of Section 2, that even in this highly linear example, the fields of increased Ri and decreased Ri are not symmetric, the maximum increase being about 4.1 and the maximum decrease about -2.6. The trapped gravity lee wave is more stabilizing than destablizing to the basic flow.

For comparison, the simulation with nonlinear terms acting is presented in Figure 2, for Case I. By 600 time steps (9000 sec) a steady state has been achieved in the grid, the computational radiation boundary condition (Sharman and Wurtele, 1983) permitting the wave to be established all the way to the outflow boundary without significant reflection. Figure 2a shows the streamfunction, here with the phase determined by the position of the 100m-obstacle. The wavelength (about 20 km) in the simulation agrees with the analytic solution of Figure 1a. Figure 2a shows a similar agreement of the vertical velocity fields, where the analytic solution has a maximum of 0.4 m/s and the simulation, 0.5 m/s, both attained at an elevation of 3 km. Whether this is scaled by the surface mean wind speed of 10 m/s or the mean speed at 3 km of about 21 m/s, the perturbation must be considered small. However, in Figure 2c, corresponding precisely to Figure 1d, we see the same lack of symmetry in the Ri-field exhibited by the analytic solution. The simulation Richardson number changes are about the same as those obtained by analysis. Here the greatest increase in Ri is about 2.8 and the greatest decrease is about -1.6.

We may now consider Case II, for which N and U are the same as in Case I, but H = 500 m. Hence Ri_o = 8, as before, but NH/U = 0.5. Here one would expect to see the linear result of Case I amplified, by a factor of about five, but with no significant nonlinear effects. And this is, in fact, what we find, in all fields except that of the Richardson number. Figures 3a,b,c,d present, respectively, the stream function, vertical velocity, horizontal velocity and Ri-field for the analytic solution of Case II. The larger disturbance shows more clearly the close correspondance between the maximum shear (Fig. 3c) and the minimum Richardson number, and vice versa. For Case II, the analytic Ri-field is highly asymmetric and varies between 3.2 and 32.

Figures 4a,b,c show the simulation fields for Case II. Again the stream function field (Figure 4a) is in agreement with the linear analytic solution. However, the most convincing quantitative evidence of linearity is in the vertical motion fields of Figs 1b, 2b, 3b and 4b. The forcing, as we have seen, increases from Case I to Case II by a factor of five. The linear solutions (Figs. 1b, 3b), not surprisingly, show an increase of the maximum amplitude of vertical velocity from 0.4 to 2.0 m/s. The simulations (Figs. 2b, 4b) show a corresponding increase from 0.5 to 2.7 m/s. In contrast, the Richardson number field (Figure 4c) shows strong nonlinearity. The positive cells are much larger in size than the negative cells, and the field varies from a maximum of 111 to a minimum of about 1.5. The nonlinear dynamics of the simulation, although not evident in the other fields, has enhanced the asymmetry of the analytic solution for the Richardson number field of Fig. 3d. As we have noted, this enhancement did not occur in the highly linear Case I.

Although the Richardson number of the basic flow determines the dimensionless wave length, other quantities, both dimensional and nondimensional (including dimensional wave length) will vary with stability and shear, even though the basic Richardson number is fixed. As an illustration of this we consider Case III, for which $N_0 = 0.5 \times 10^{-2} s^{-1}$, L = 5.66 km and H = 500 m. Thus $Ri_o = 8$, as in Cases I and II, but both shear and stability have been decreased by a factor of two.

Figure 5 (a,b,c,d) displays the fields from the linear analysis for Case III. The dimensional wave length has increasd to about 42 km. The level of trapping has also increased; this is most evident in the vertical velocity field Figure 5b, where the maximum is centered at about 7 km elevation, instead

of at 3 km for Cases I and II. Since the level of trapping is higher, the energy from the forcing is supplied to a larger volume of atmosphere, and the disturbance amplitude is correspondingly smaller.

So far we have discussed conditions permitting a single trapped wave. In order to limit the system to a single free mode, it was necessary to specify a relatively small Richardson number by atmospheric standards, $Ri_o = 8$. Reference to Appendix A and to Figure A1 show that doubling this value to $Ri_o = 16$ defines a condition in which two free modes are admissible, of wavelengths approximately 15 km and 30 km. To define Case IV then, we take $N = 10^{-2} s^{-1}$, $L = 4$ km, and $H = 500$ m. Thus $Ri_0 = 16$ and $NH/U = 0.5$. As with Case II, we shall see that all fields except that of the Richardson number exhibit linear behavior.

Figure 6 (a,b,c,d) displays the fields corresponding to those of Figures 1,3 and 5, that is, the stream function, vertical velocity, total horizontal velocity, and total Richardson number for the first mode only. The patterns are the familiar ones from The $Ri_0 = 8$ cases. And the same is true of Figure 6 (a,b,c,d) containing the corresponding representations for the second mode only. The second mode, of course, has two cells in the vertical in the streamfunction, vertical velocity, and Richardson number fields, and three cells in the horizontal velocity field. This mode has its maximum amplitude at a higher level than the first mode velocity fields, but the maximum are less than those of the first mode. Richardson number in each mode is reduced by slightly more than 50% in the centers of the negative cells.

The total linear free-wave solution is the sum of these two modes, presented in Figure 8 (a,b,c). The perturbation stream function field of Figure 8a shows clearly the superposition of a short and long wave, the former

dominating at lower, and the latter at higher elevations. The same is true of the vertical velocity field of Fig. 8b. Yet the wavelengths of the two waves - derived, it will be recalled, as roots of a Bessel function - are not of integral ratio, and thus the combined pattern is not strictly periodic. In the figure, there is a maximum value for w of about 2.3 m/s. Thus the problem is within the bounds of linearity, and the fields of these two figures have an ordered pattern.

The Richardson number field (Fig. 8c), however, is complex and the pattern would be difficult to anticipate. The maximum Richardson number in the graphed portion of the field is of the order of 10^6, but the minimum, 3.1, is greater than the minima of the two modes separately.

4. Limits of linearity

For the trapped lee wave, as the wind shear increases, the level of trapping is displaced downward, and wave amplitudes are increased. As the amplitude becomes larger, nonlinear effects may be expected to become more significant. As an illustration of this we consider Case V, for which we choose $N = 2 \times 10^{-2} s^{-1}$, L = 1.414 km and H = 500 m. Thus $Ri_o = 8$, as in Cases I and II, but both shear and stability have been increased by a factor of two. And NH/U = 1, also twice the value of Case II. The Figure 9 (a,b,c,d) shows clearly the increased magnitude of all quantities. The maximum vertical velocity is now 32% of U and the minimum Richardson number is 0.51, approaching the critical. However, traditionally a value of unity for NH/U would be said to render a linear analysis invalid, and we must at this point consider the problem of criteria for nonlinearity.

We first note that the conventional parameter of linearity, NH/U, developed for uniform flow when these three parameters determine the flow completely, is less easy to justify when shear is present. Another length, L, is available, and H/L would seem to be a candidate dimensionless parameter of the problem. The most thorough perturbation analysis of shear flow is that developed by Brown and Stewartson (1982) for an essentially nonlinear problem, that of a gravity wave propagating toward a critical level. Although the forcing in their problem is not specified, if it is identified with kinematic forcing at a lower (or upper) boundary, their expansion parameter can be identified as our H/L. From equation (12) we have an expression for the vertical velocity w :

$$\frac{w}{U} = -2 \pi (ak_1) e^{-ak_1} \frac{H}{L} \frac{K_{i\mu}(\kappa_1 Z)}{K'_{i\mu}(\kappa_1)} \cos k_1 x$$

It is evident here that H/L is the ratio determining the amplitude, and that the stability, as represented by N_0, plays little role. It is true that the quantity

$$(ak_1) \exp (-ak_1) \ ,$$

associated with the shape of the forcing obstacle, is a function of N_0, but it is not a monotonic function, and its maximum value is e^{-1}.

Thus in general we have the results that NH/U is the amplitude parameter for the zero-shear case and H/L, or more generally, $\frac{H}{u_0} \frac{d u_0}{dz}$, is the amplitude parameter for a shear flow. However, we cannot pretent that the problem has been solved. In the first place, the shear flow must depend on some combination of these parameters; otherwise $L \to \infty$ (shear approaching zero) gives a wrong result. The failure of the criterion for shear flow to pass into the corresponding result for zero-shear flow is characterstic of all theoretical formulations.

In the second place, what does "nonlinearity" mean in this context. In lee wave theory it has been taken to mean $u' \rightarrow -u_0$, $\partial \rho / \partial z \rightarrow 0$, i.e., overturning and wavebreaking. In order to examine the consequences of such a situation, we have used a simulation code better adapted to extreme nonlinear parameter-space, that of Pihos and Wurtele (1981). In Figures 10-12a, b, we present the streamline pattern and density contours for $Ri_0 = 8$, under conditions of Case V, except that NH/U takes on the values of 1.0, 1.5, and 3.0, respectively. We see that (1) overturning - as evidenced by heavier fluid above lighter - is not present until NH/U = 3; and (2) even at this value, the instability is highly local and does not spread with increasing time. In fact, the choice of values to be plotted in the streamline field fails to resolve the overturning at all.

For all these three runs, the value of L is 4 km, so that H/L is 0.174, 0.265 and 0.530 respectively. The beginnings of instability for this last value suggests that H/L is the decisive dimensionless parameter for stratified shear flows.

As a control, we submit the experiment of Figure 13, in which there is zero shear, i.e. U = constant, N = constant. In this case, as indicated above, the parameter NH/U governs linearity, and the value of unity assigned to it in this run has clearly produced overturning.

5. Nonlinear Analysis

It is not clear that a linear (or perturbation) analysis is the best or only possible approach to this problem. Some light is cast by following a line begun by Scorer (1969), using one Lagrangian coordinate, say, potential temperature. The transformation equations - somewhat more complicated than in the hydrostatic model - are listed for convenience in Appendix B. We consider only the steady-state, in which isentropes are streamlines. We thus have from (B5), the equation of continuity, and (B6), the vorticity equation, in terms of the total (finite) variables:

$$\frac{\partial}{\partial x}\left(u \frac{\partial z}{\partial \theta} \right) = 0 \, , \tag{13}$$

where z is the height of an isotropic surface or streamline, and

$$u \frac{\partial \zeta}{\partial x} = - \frac{g}{\theta} \left(\frac{\partial z}{\partial \theta} \right)^{-1} \frac{\partial z}{\partial x} \tag{14}$$

where ζ is the vorticity. The first of these may be integrated to yield, using (B3),

$$\frac{u}{u_0} = \frac{N^2}{N_0^2} \tag{15}$$

where U_0 and N_0 are values far upstream on the streamline, both functions of height. This equation simply quantifies our intuitive knowledge that when a streamline becomes vertical (u = 0), the stability also vanishes. This is not in general the case in linear analysis, if we identify $u_0 + u'$ with u and $N_0^2 - \partial \sigma'/\partial z$ with N^2. From (1) to (3) we obtain in contrast to (15),

$$\frac{N^2}{N_0^2} = \frac{u}{u_0} - \frac{\psi'}{N_0^2}\frac{\partial}{\partial z}\left(\frac{N_0^2}{u_0}\right)$$

This equation illustrates the familiar result that linear solutions satisfy the nonlinear equations provided $\frac{N_0^2}{u_0}$ is constant. For the model of Section 2,

$$\frac{N^2}{N_0^2} = \frac{u}{u_0} + \frac{\psi'}{UL}\left(1 + \frac{z}{L}\right) .$$

This will, in general, occur in a finite layer, with $\frac{\partial u}{\partial z}$ and N^2 both near zero or negative, emphasizing that when convective instability enters the problem, the Richardson number ceases to be a useful concept.

We may gain a little further insight from the vorticity equation (B6), again using (B3)

$$u\frac{\partial \zeta}{\partial x} = -N^2\frac{\partial z}{\partial x} .$$

Since by (15) the ratio N^2/u is constant along a streamline, this may be integrated to yield

$$\frac{u_0}{N_0^2}(\zeta - \zeta_0) = -(z - z_0) = -\delta$$

where δ is the vertical displacement of a streamline. Qualitatively this equation states that (in this right-handed system) the vorticity increases when the streamline is depressed and decreases when it is lifted; but it further states that the change is linear with streamline displacement and specifies the constant of proportionality for each streamline.

6. Conclusions

An analytic solution has been presented for a stratified fluid of arbitrary constant Richardson number. By computer aided analysis the perturbation fields, including that of the Richardson number can be calculated. The results of the linear analytic model were compared with non-linear simulations, leading to the following conclusions.

1. The perturbations in the Richardson number field, when small, are produced primarily by the perturbations of the shear.

2. Perturbations of in the Richardson number field, even when small, are not symmetric, the increase being significantly larger than the decreases. The linear analytic solution and the nonlinear simulations both confirm this result.

3. As the perturbations grow, this asymmetry increases, but more so in the nonlinear simulations than in the linear analysis.

4. For large perturbations of the shear flow, the static stability, as represented by N^2, is the dominating mechanism, becoming zero or negative, and producing convective overturning.

5. The convectional measure of linearity in lee wave theory, NH/U, is no longer the critical parameter. It is suggested that $\dfrac{H}{u_0} \dfrac{du_0}{dz}$ takes on this role in a shearing flow.

ACKNOWLEDGMENTS

REFERENCES

Abramowitz, M. and I.A. Stegun, 1964: Handbook of Mathematical Funtions, Nat. Bur. Standards, Ap. Math. Ser.55.

J.R. Booker and F.P. Bretherton, 1967: "The critical level for internal gravity waves in a shear flow," J. Fluid Mech, 27, 513-530

Brown, S.N. and K. Stewartson, 1982: "On the nonlinear reflection of a gravity wave at a critical level, Part 2," J. Fluid Mech., 115, 217-230.

Foldvik, A., and M.G. Wurtele, 1967: "The computation of the transient gravity wave," Geophys. J.R. Astr. Soc., 13, 167-185.

Fritts, D.C., 1979: "The excitation of radiating waves and Kelvin-Helmholtz instabilities by gravity wave - critical level interaction," J. Atmos. Sci., 36, 12-23.

Gossard, E.E. and W.H. Hooke, 1975: Waves in the Atmosphere, Elsevier Scientific Pub. Co., 456 pp.

Hodges, R.R., 1967: "Generation of turbulence in the upper atmosphere by internal gravity waves," J. Geophys. Res., 72, 3455-3458.

Jahnke, E., and F. Emde, and F. Losch, 1960: Tables of Higher Functions, McGraw Hill Book Co., 318 pp.

Keller, T.L., M.G. Wurtele, and L.J. Ehernberger, 1983: "Numerical simulation of the atmosphere during a CAT encounter," Proc. Ninth Conf. Aerospace/Aeronautical Meteor., Amer. Meteor Society, Omaha, June, 1983.

Lamb, H., 1932: Hydrodynamics, sixth ed., Cambridge Univ. Press, 738pp.

Lindzen, R.S., 1981: "Turbulence and stress owing to gravity wave and tidal breakdown," J. Geophys. Res., 86, 9707-9714.

Miles, J.W., 1968: "Lee waves in a stratified flow, Part 2," J. Fluid Mech., 33, 803-814 (with an Appendix by H.E. Huppert).

Mowbray, D.E., and B.S.H. Rarity, 1967: "A theoretical and experimental investigation of the phase configuration of internal waves of small amplitude in a density stratified fluid," J. Fluid Mech., 28, 1-16.

Morgan, S.P. 1947: "Tables of Bessel Functions of imaginary order and imaginary argument," California Institute of Technology, Pasadena.

Palm, E., and A. Foldvik, 1960: "Contribution to the theory of two-dimensional mountain waves," Geofy. Publ., Vol. 21, no. 6, pp. 1-30.

Pihos, G.G. and Wurtele, M.G. 1981: "An efficient code for the simulation of nonhydrostatic stratified flow over obstacles," NASA CR 3385.

Queney, P., G. Corby, N. Gerbier, H.Koschmieder and J. Zierep, 1960: The airflow over mountains, Tech. Note 34, World Meterological Organization, Geneva.

Scorer, R.S., 1949: "Theory of waves in the lee of mountains," Quart. J. Royal Meteor. Soc., 76, 41-56.

Scorer, R.S., 1969: "Mechanisms of clear air turbulence," in Clear air turbulence and its detection, ed. Y.H. Pao and A. Goldburg, Plenum Press, 542pp.

Sharman, R.D., 1981: "Three-dimensional lee waves in a continuously stratified fluid," Ph.D. dissertation, University of California, Los Angeles, 151 pp.

Sharman R.D. and M.G. Wurtele, 1983: "Ship waves and lee waves," J. Atmos. Sci., 40, 396-427.

Smith, R.B., 1977: "The steepening of hydrostatic mountain waves," J. Atmos. Sci., 34, 1634-1654.

Thorpe, S.A., 1981: "An experimental study of critical layers," J. Fluid Mech., 103, 321-344.

Wurtele, M.G., 1953: "Studies of lee waves in atmospheric models with continuously distributed static stability," Scientific Report No. 4, Contract No. AF19(122)-263, U.C.L.A.

Wurtele, M.G. and R.D. Sharman, 1983: "Numerical and analyical investigations of three-dimensional lee waves," Proc. Ninth Conf. Aerospace/Aeronautical Meteor., Amer. Meteor. Soc., Omaha, June, 1983.

TABLE I

Case	Figure	$N(s^{-1})$	$U(m/s)$	$L(km)$	Ri_0	$H(km)$	NH/U	H/L
I	1,2	.01	10	2.83	8	0.1	.1	.035
II	3,4	.01	10	2.83	8	0.5	.5	.177
III	5	.005	10	5.66	8	0.5	.25	.088
IV	6,7,8	.01	10	4.00	16	0.5	.5	.125
V	9,10	.02	10	1.41	8	0.5	1.0	.354
VI	11	.02	10	1.41	8	0.75	1.50	.265
VII	12	.02	10	1.41	8	1.50	3.00	.530
VIII	13	.02	10	∞	∞	0.50	1.00	0

LEGENDS

Figure 1a. Graph of perturbation stream function from linear analysis in Case I (see Table I). All units in this and other computations are MKS.

Figure 1b. Vertical velocity from analysis for Case I. Contour interval is 0.2 m/s. In this and all subsequent figures of vertical velocity from analysis the first (leftmost) cell is negative.

Figure 1c. Total horizontal velocity from analysis for conditions of Case I. Contour interval is 2 m/s.

Figure 1d. Richardson number field from analysis for Case I contoured for the quantity $(Ri - Ri_0)/Ri_0$. The contour interval (dimensionless) is 0.05. In this and all subsequent figures of Ri from analysis the first (leftmost) cell is a region of Ri increase.

Figure 2a. Stream function in simulation for conditions of Case I, at time step 600 (9000 sec).

Figure 2b. Vertical velocity in simulation of Case I. Contour interval is 0.1 m/s. (Note that contour interval is one-half that of Fig. 1b).

Figure 2c. Richardson number field in simulation of Fig. 2a. As in Fig. 1c, the quantity contoured is $(Ri-Ri_0)/Ri_0$, and the contour interval is 0.05.

Figure 3a. Graph of perturbation stream function from linear analysis for Case II. (See Table I).

Figure 3b. Vertical velocity field from linear analysis for Case II. Contour interval is 0.2 m/s .

Figure 3c. Total horizontal velocity contours from linear analysis for Case II. Contour interval is 2 m/s .

Figure 3d.   Total Richardson number field from linear analysis for Case II.
             Contour interval is 1.0.

Figure 4a.   Graph of perturbation stream function from simulation for Case II,
             600 times steps (7200 sec).

Figure 4b.   Vertical velocity contours from simulation for Case II. Contour
             interval is 0.2 m/s.

Figure 4c.   Richardson number field from simulation for Case II. The quantity
             contoured is $(Ri-Ri_0)/Ri_0$ with a contour interval of 0.10, or
             equivalenctly total Ri with a contour interval of 0.8.

Figure 5a.   Graph of perturbation stream function from linear analysis for
             Case III (see Table I).

Figure 5b.   Vertical velocity contours from linear analysis for Case III.
             Contour interval is 0.2 m/s.

Figure 5c.   Total horizontal velocity contours from linear analysis for
             Case III. Contour interval is 2.0 m/s.

Figure 5d.   Total Richardson number field from linear analysis for Case III.
             Contour interval is 1.0.

Figure 6a.   Graph of perturbation stream function from linear analysis for
             Case IV (see Table I). First mode only.

Figure 6b.   Vertical velocity contours from linear analysis for Case IV, first
             mode only. Contour interval is 0.2 m/s.

Figure 6c.   Total horizontal velocity contours from linear analysis for Case IV
             first mode only. The contour interval is 2 m/s.

Figure 6d.   Total Richardson number field from linear analysis for Case IV,
             first mode only. The contour interval is 2.0.

Figure 7a.   Same as Fig. 6a, but for second mode only.

Figure 7b.   Same as Fig. 6b, but for second mode only.

Figure 12b. Total density field corresponding to Figure 12a.

Figure 13.   Stream function at 400 time steps (4000 sec) as simulated by the non-linear gravity wave code by Pihos and Wurtele (1981) for Case VIII (see Table I).

Figure 1a
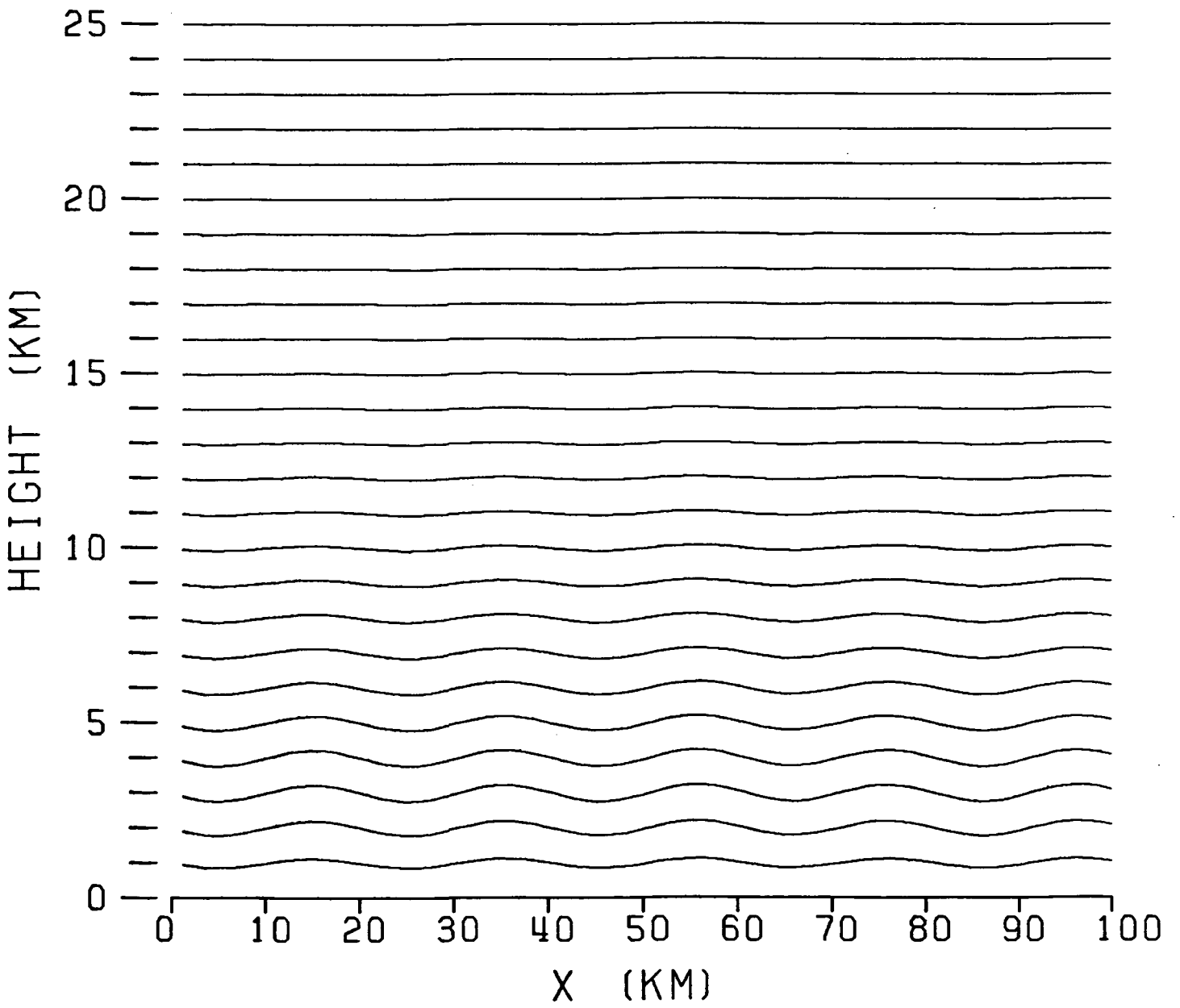
Figure 1b
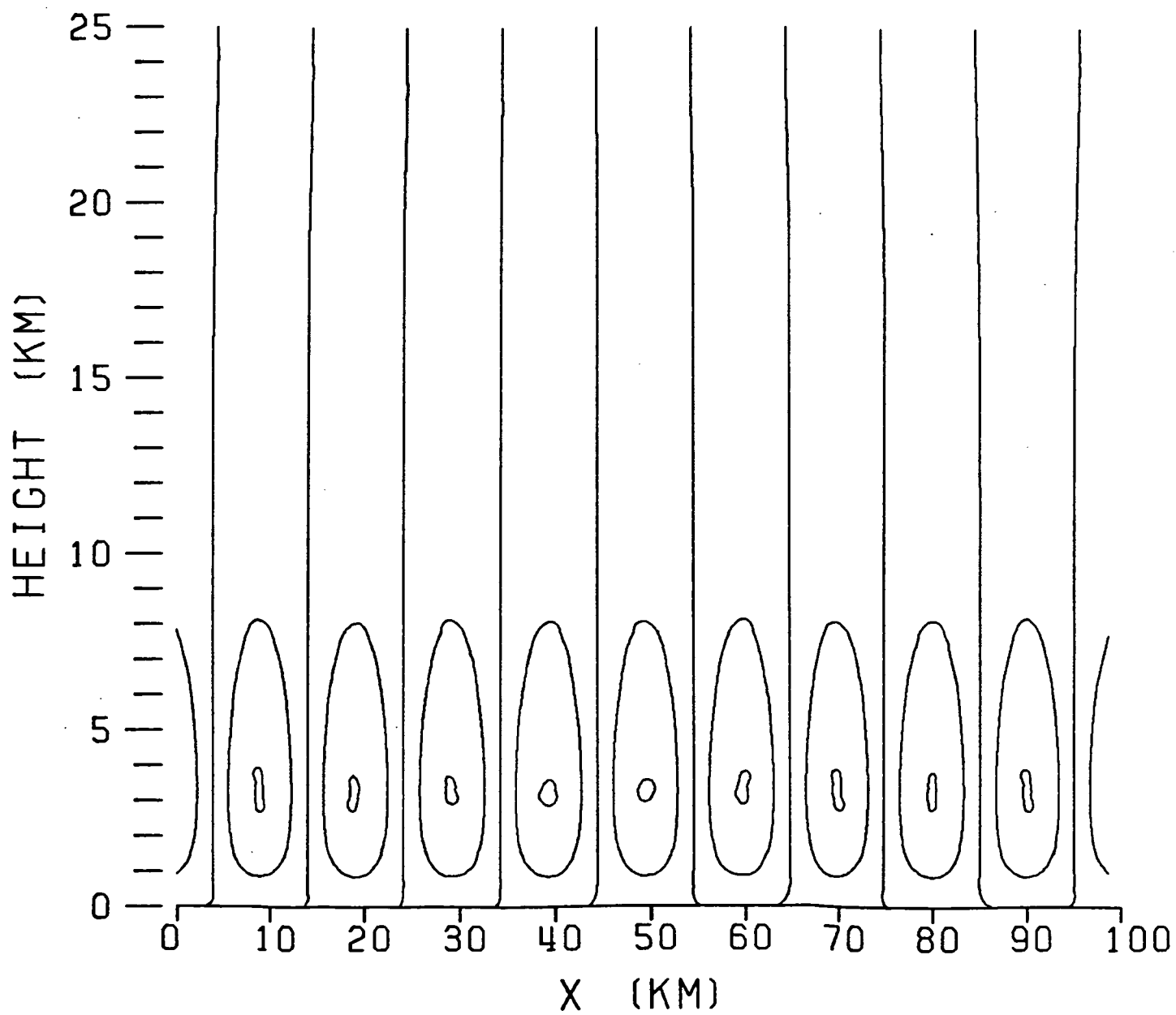
Figure 1c
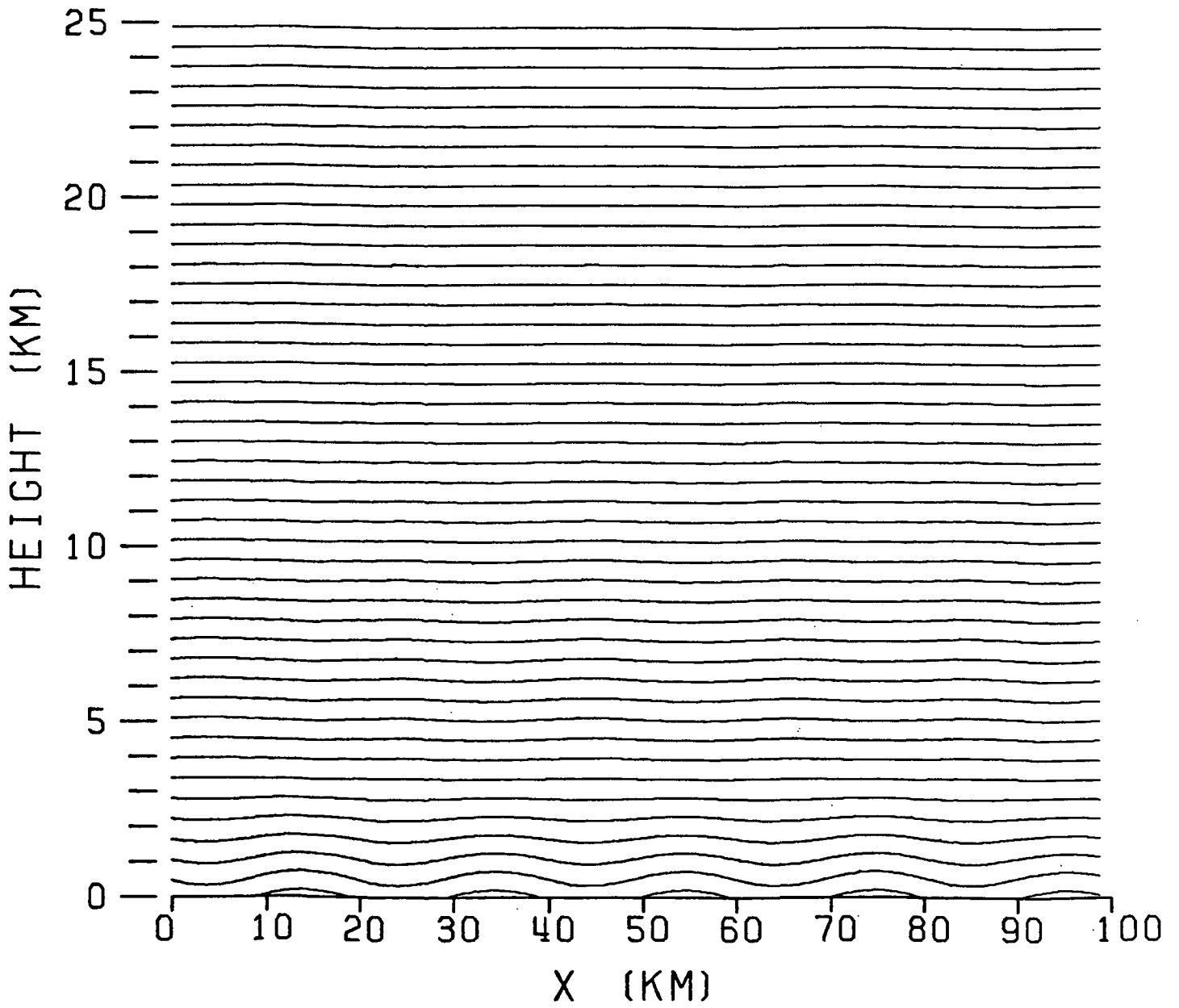
Figure 1d
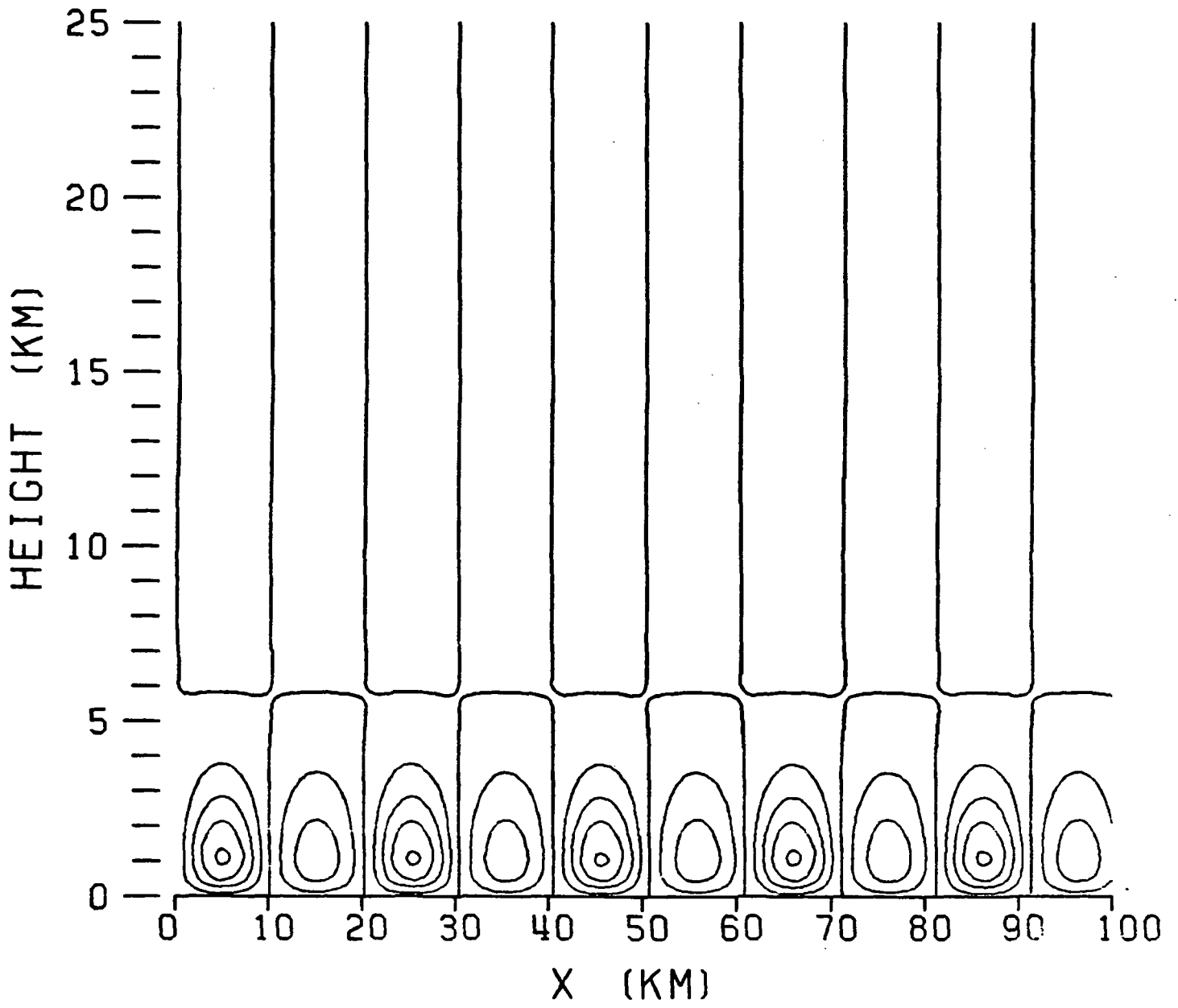
Figure 2a
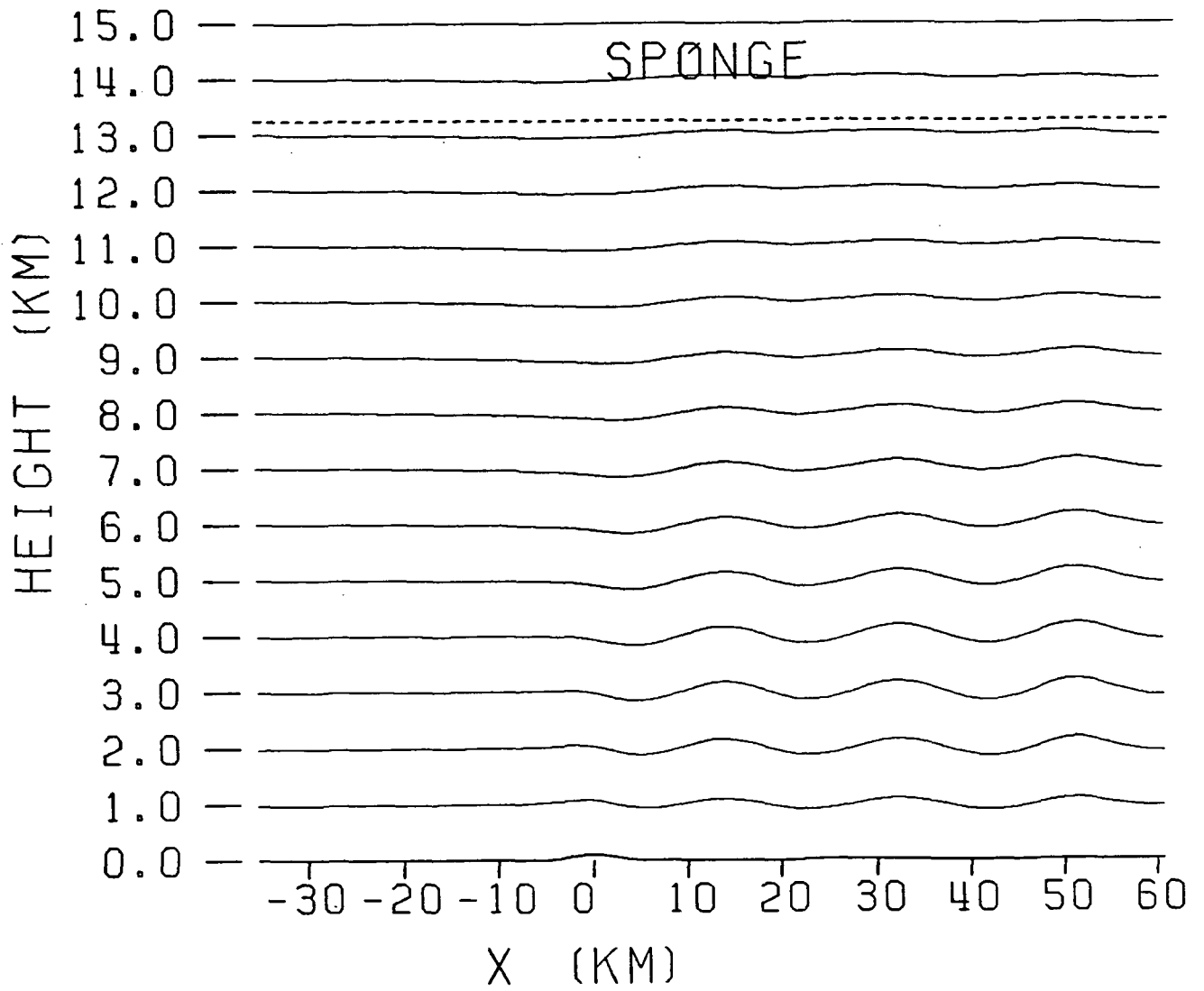
Figure 2b
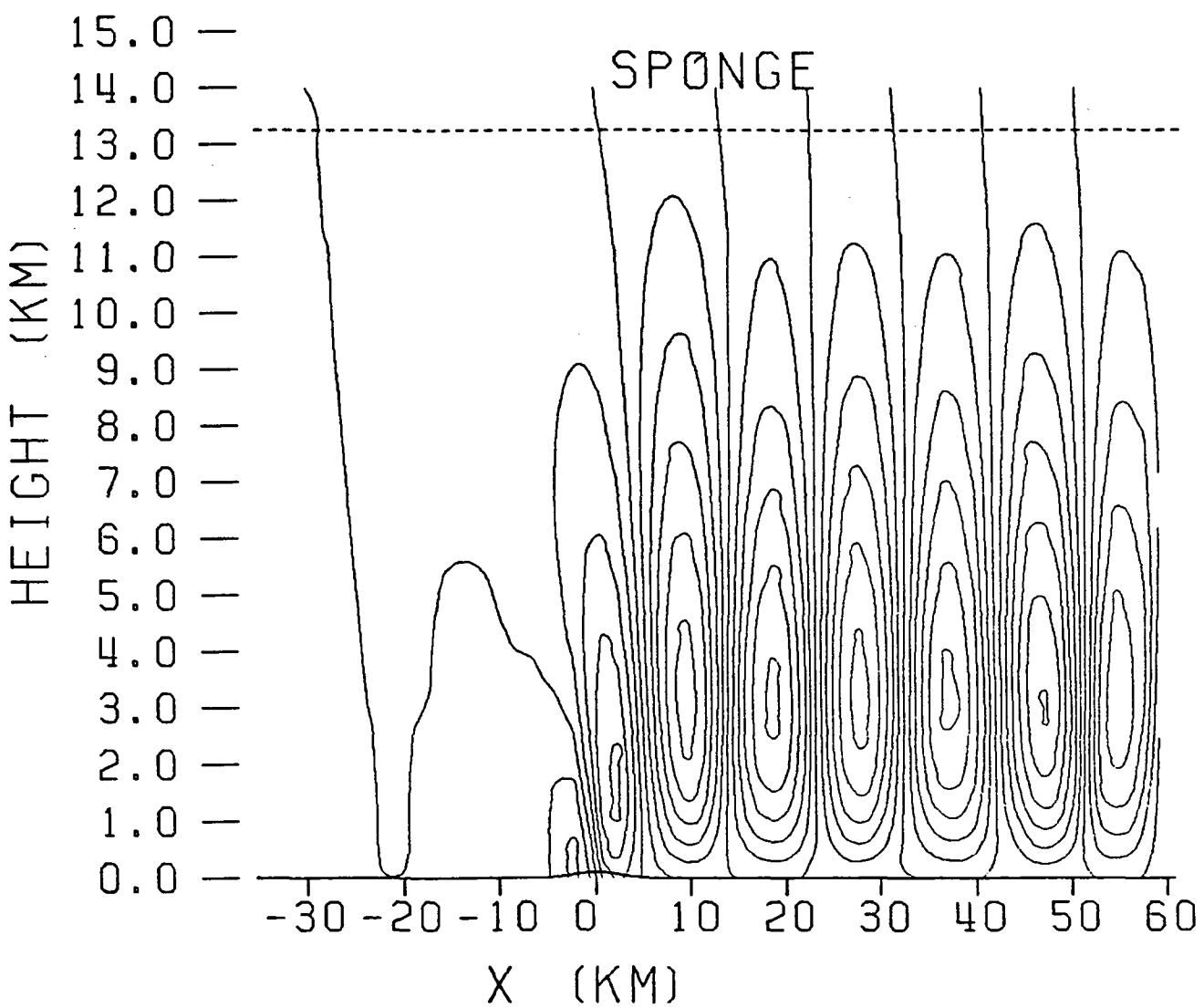
Figure 2c
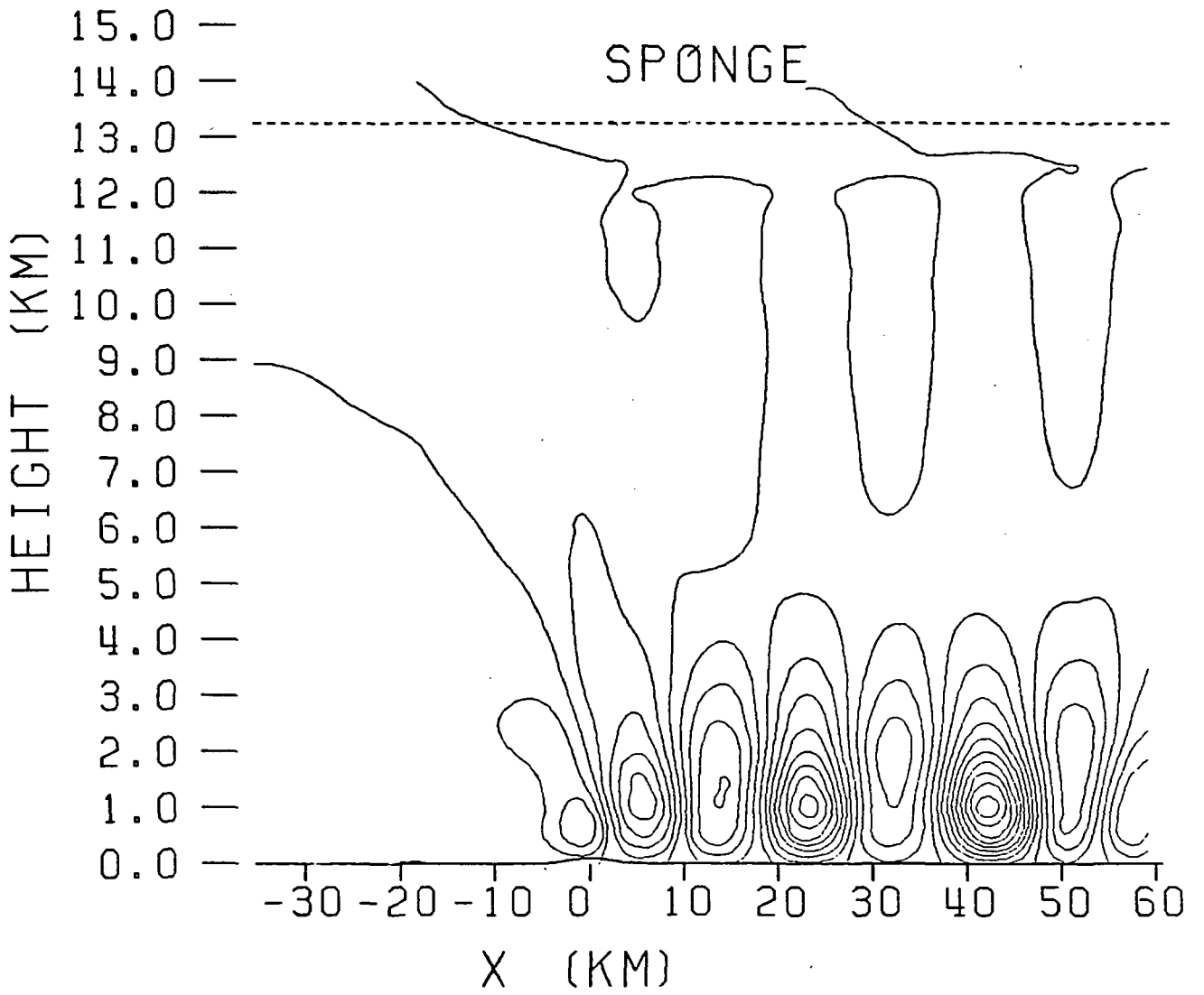
Figure 3a
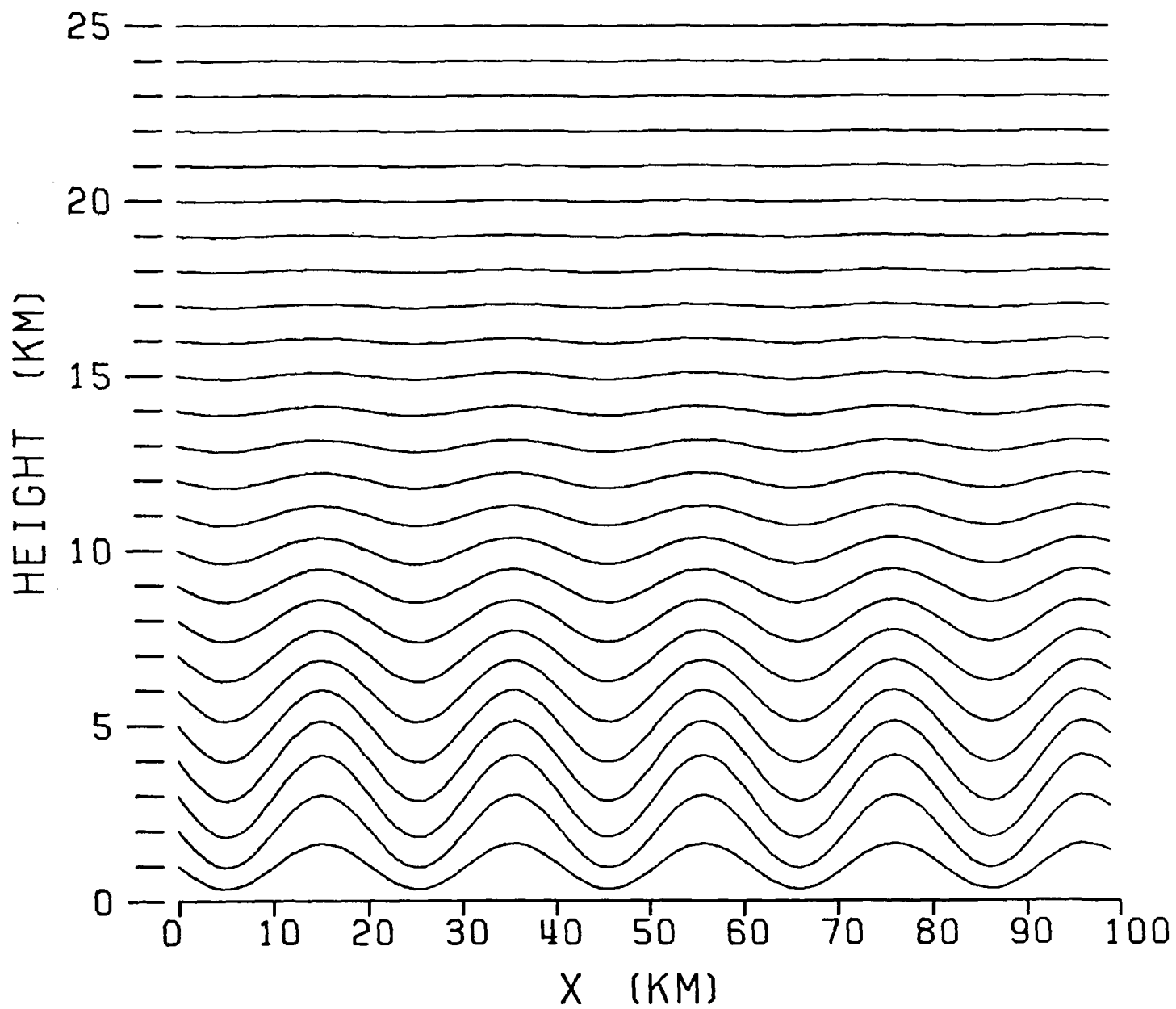
Figure 3b
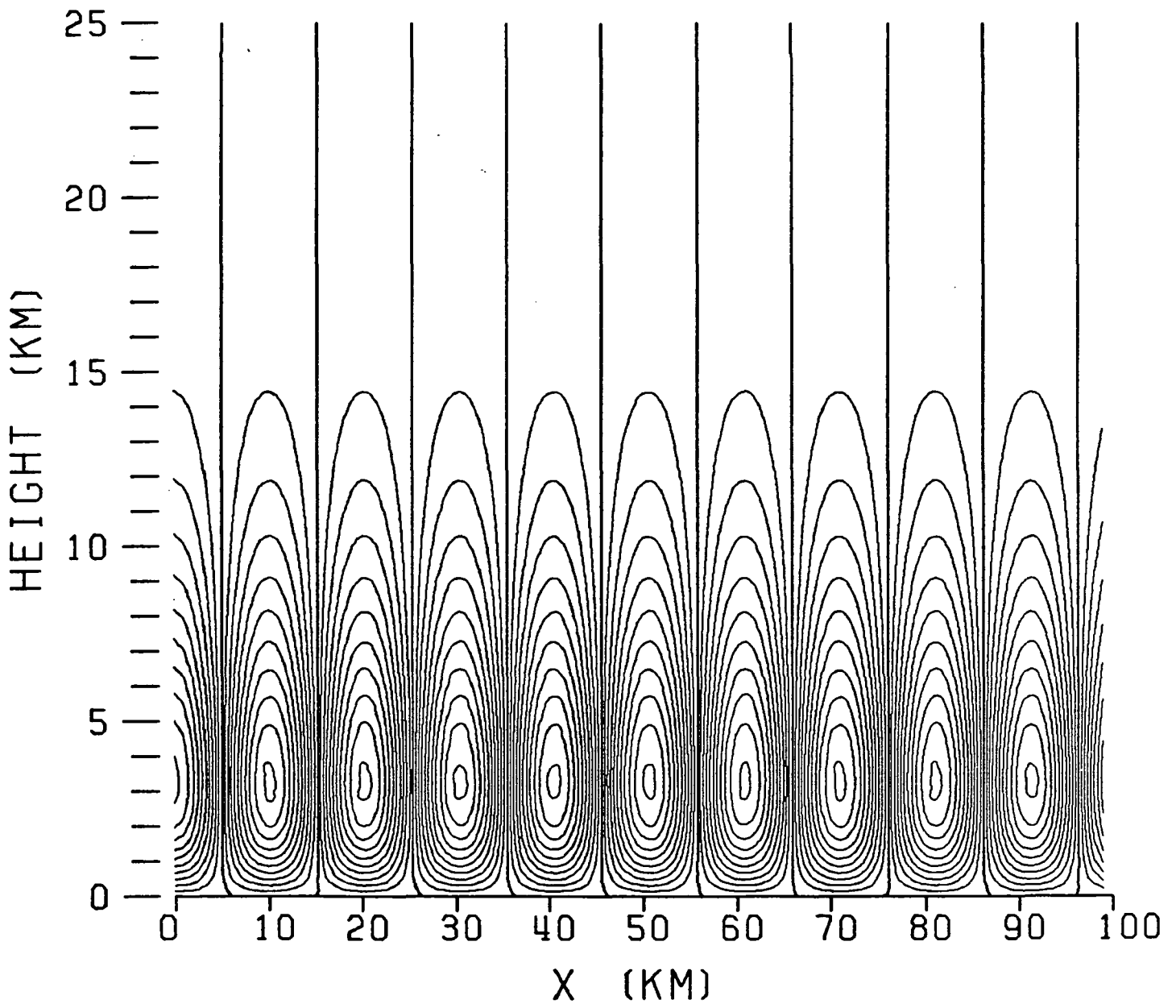
Figure 3c
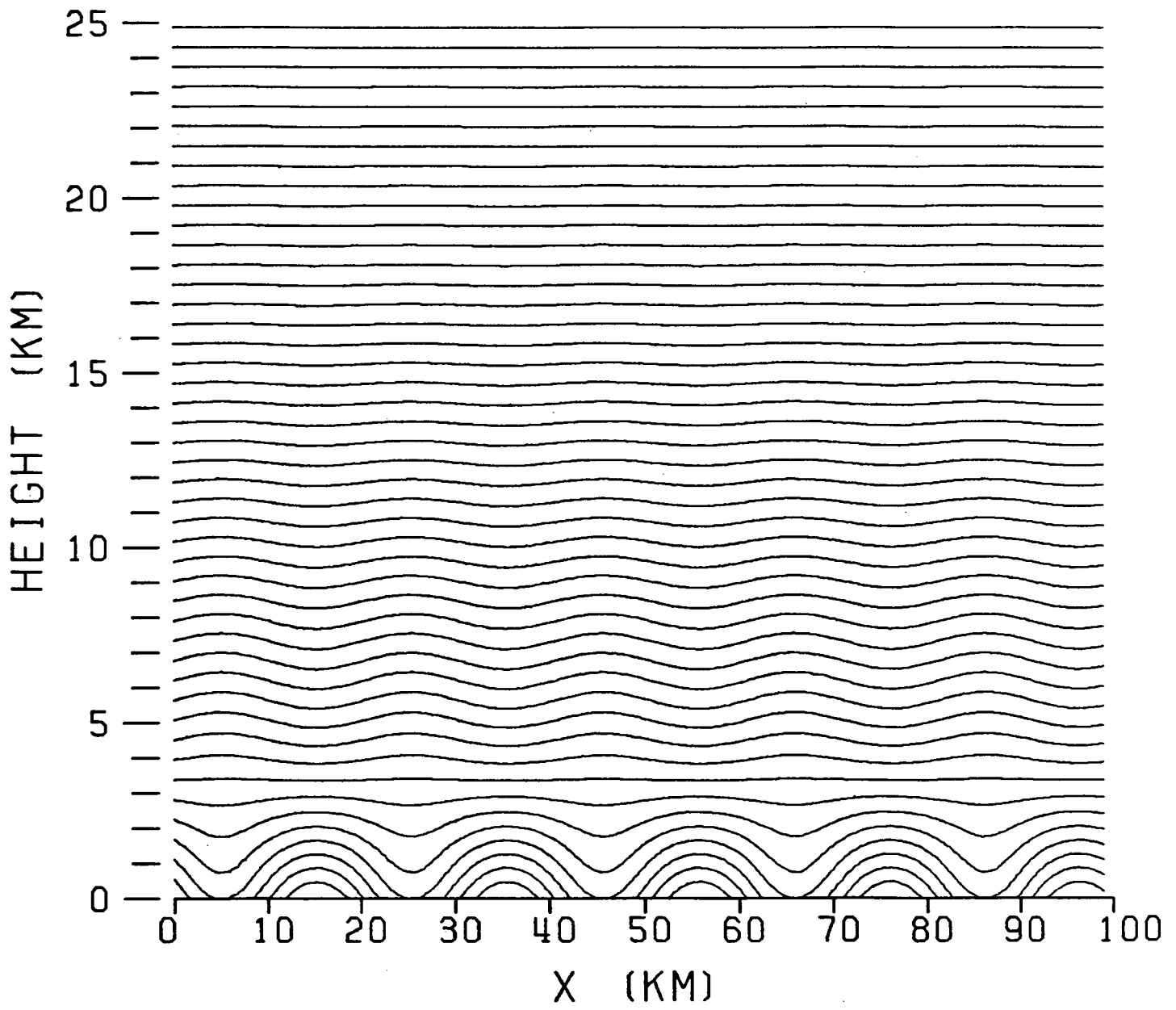
Figure 3d
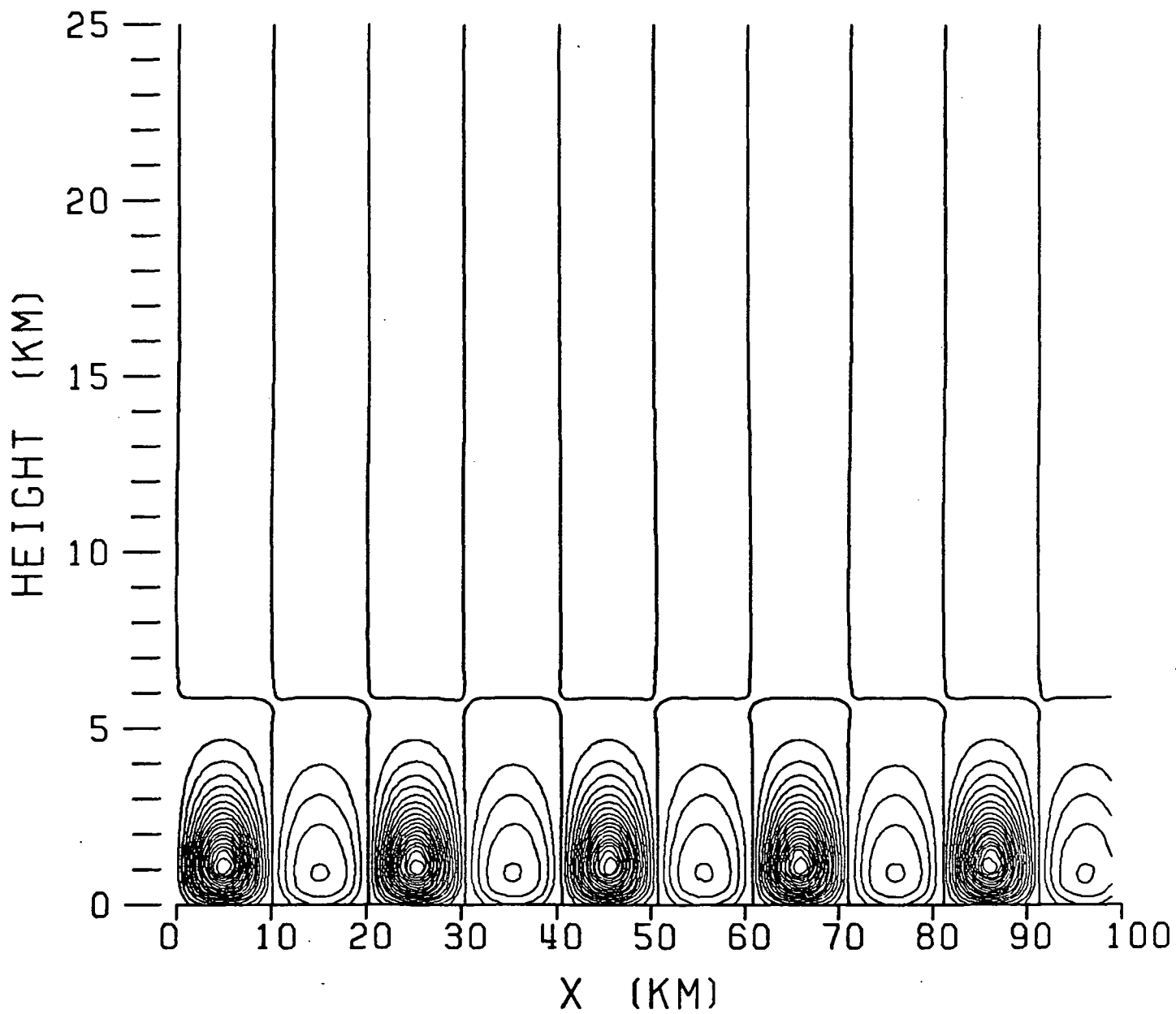
Figure 4a
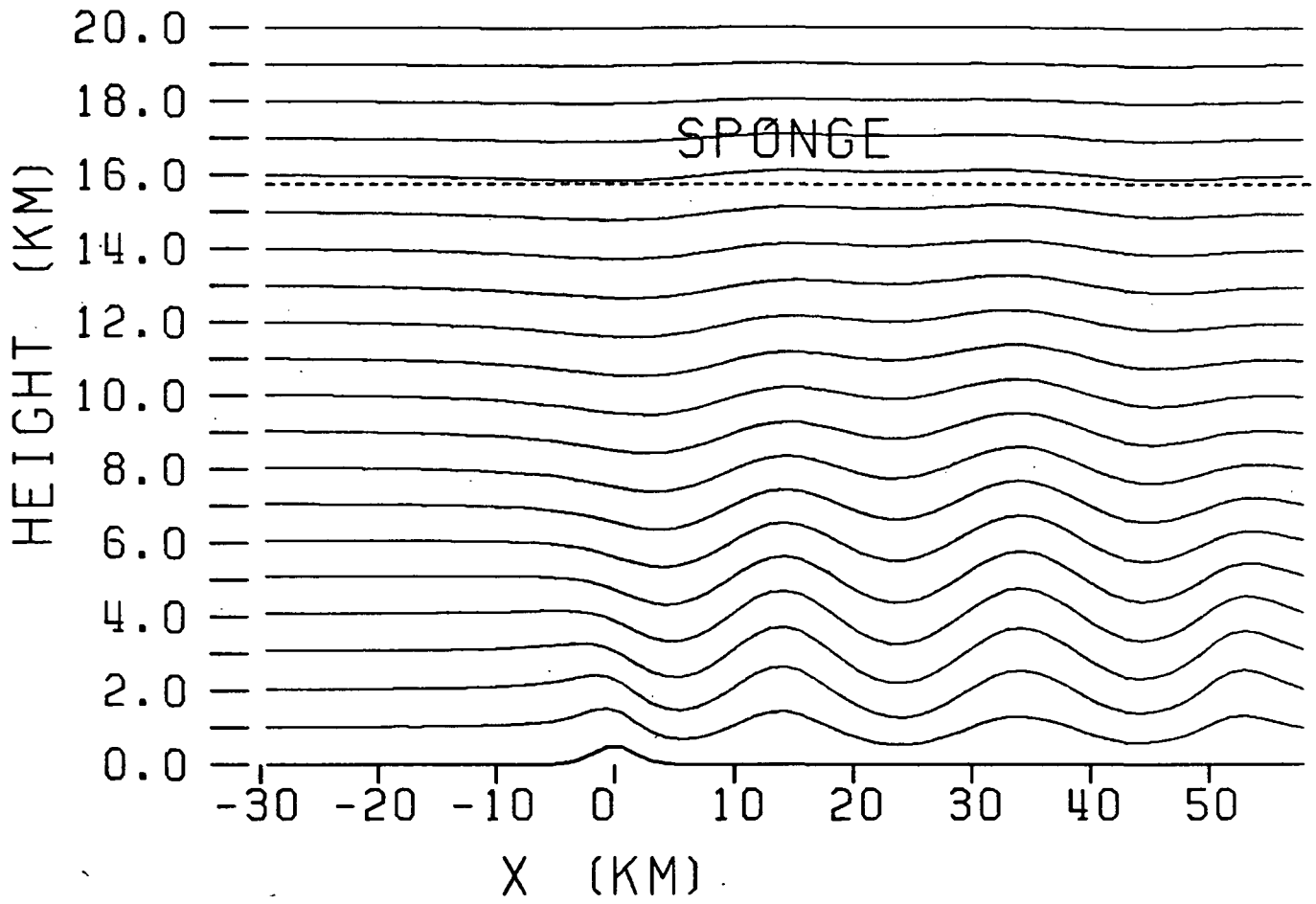
Figure 4b

figure 4c
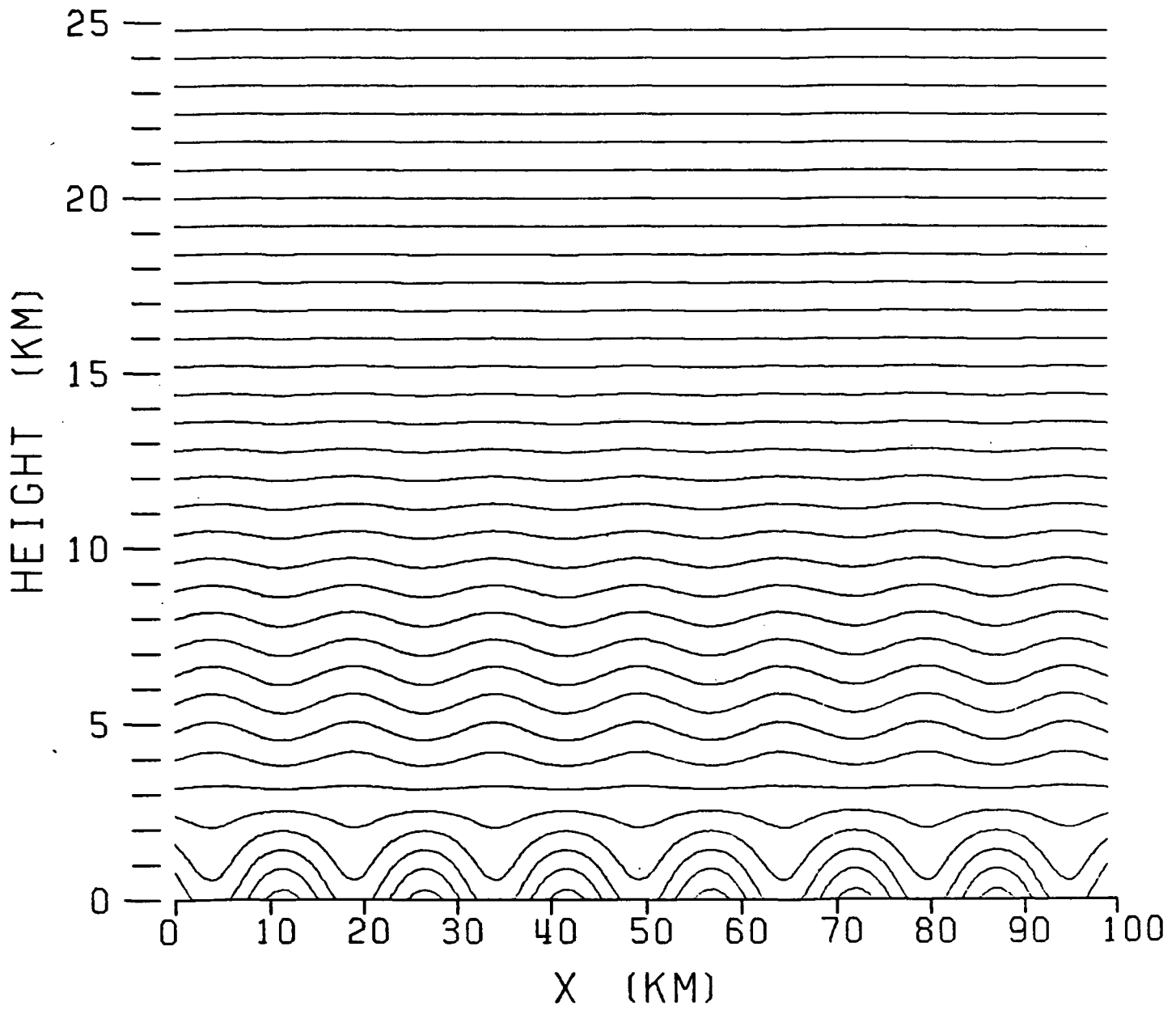

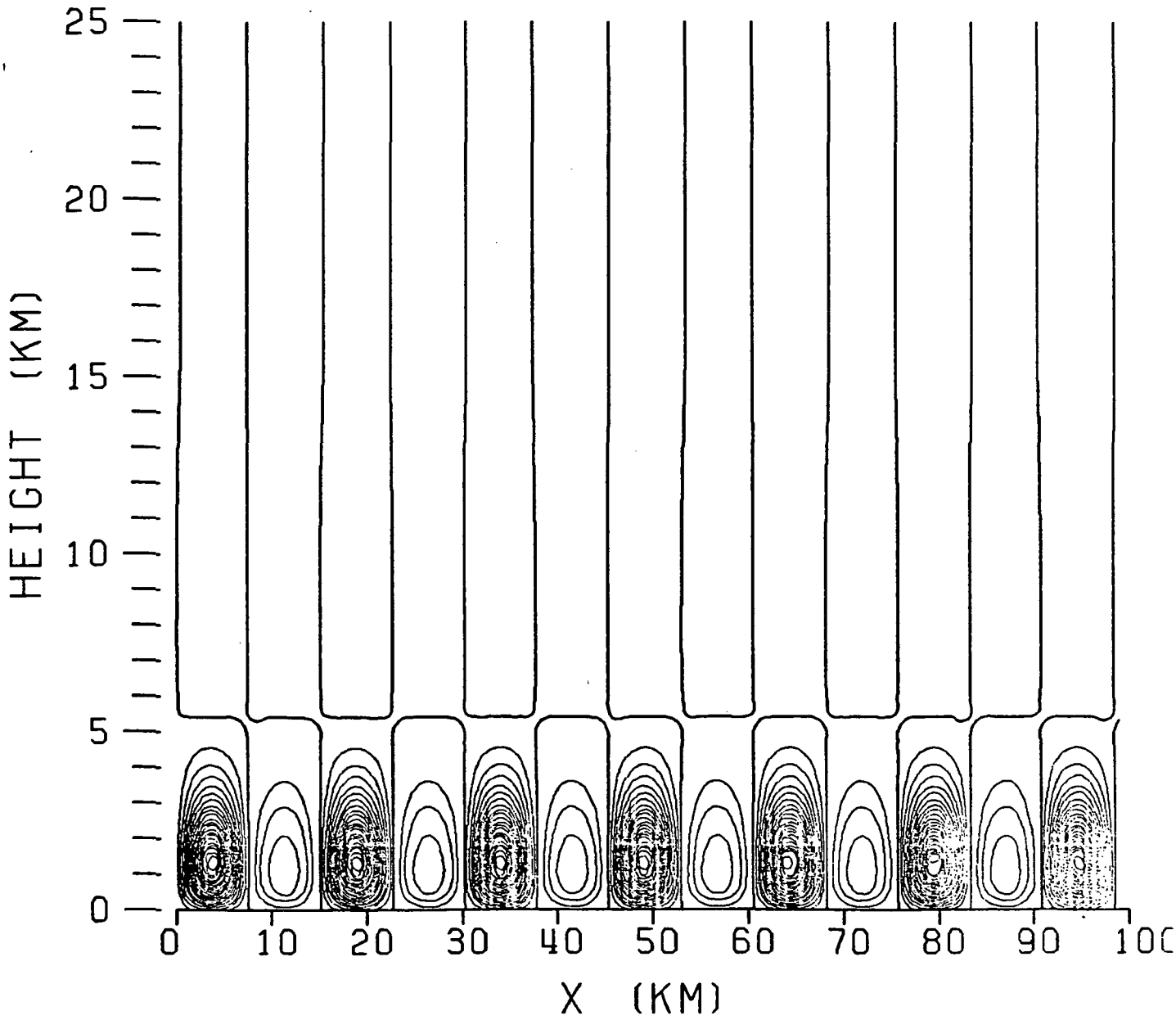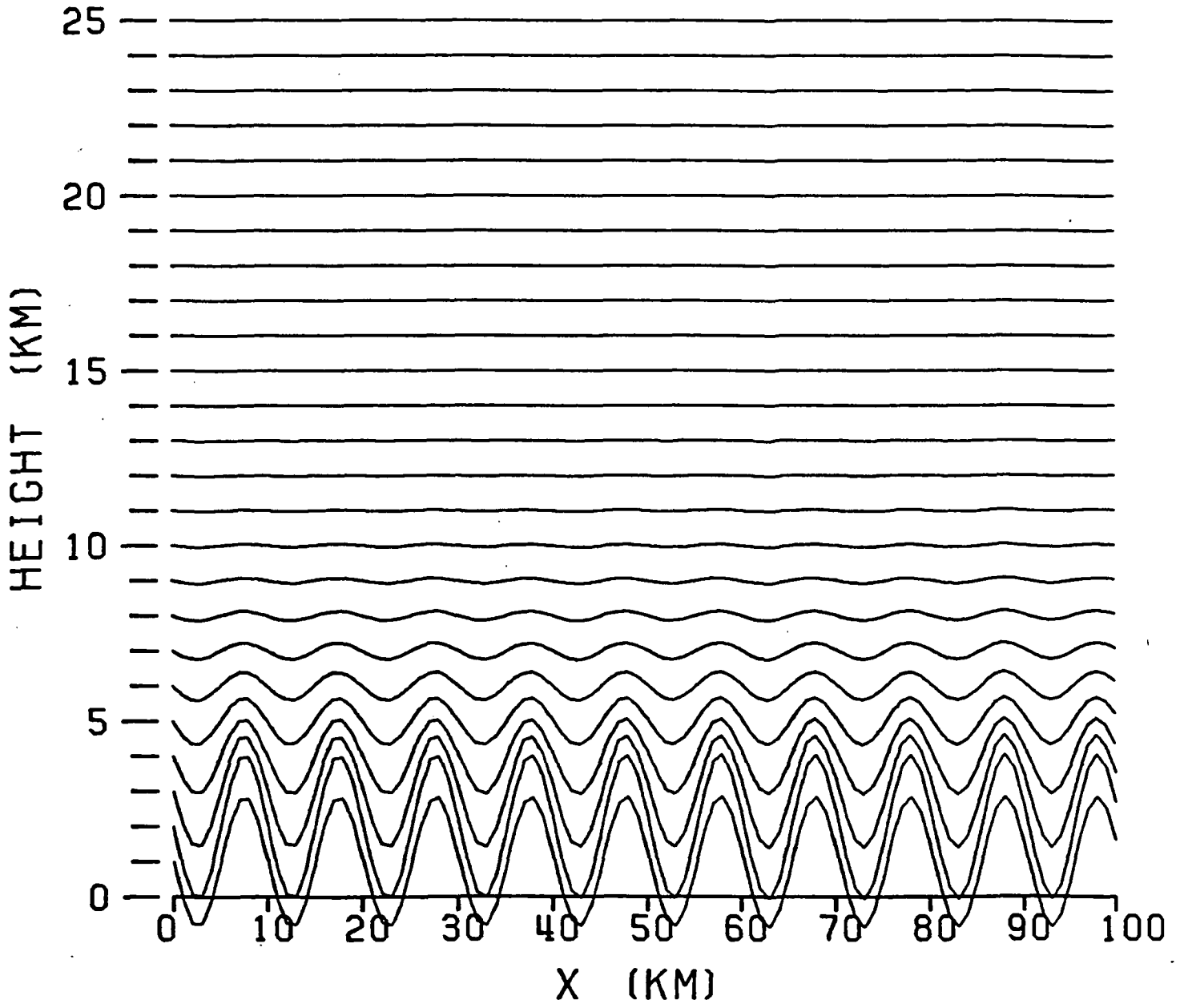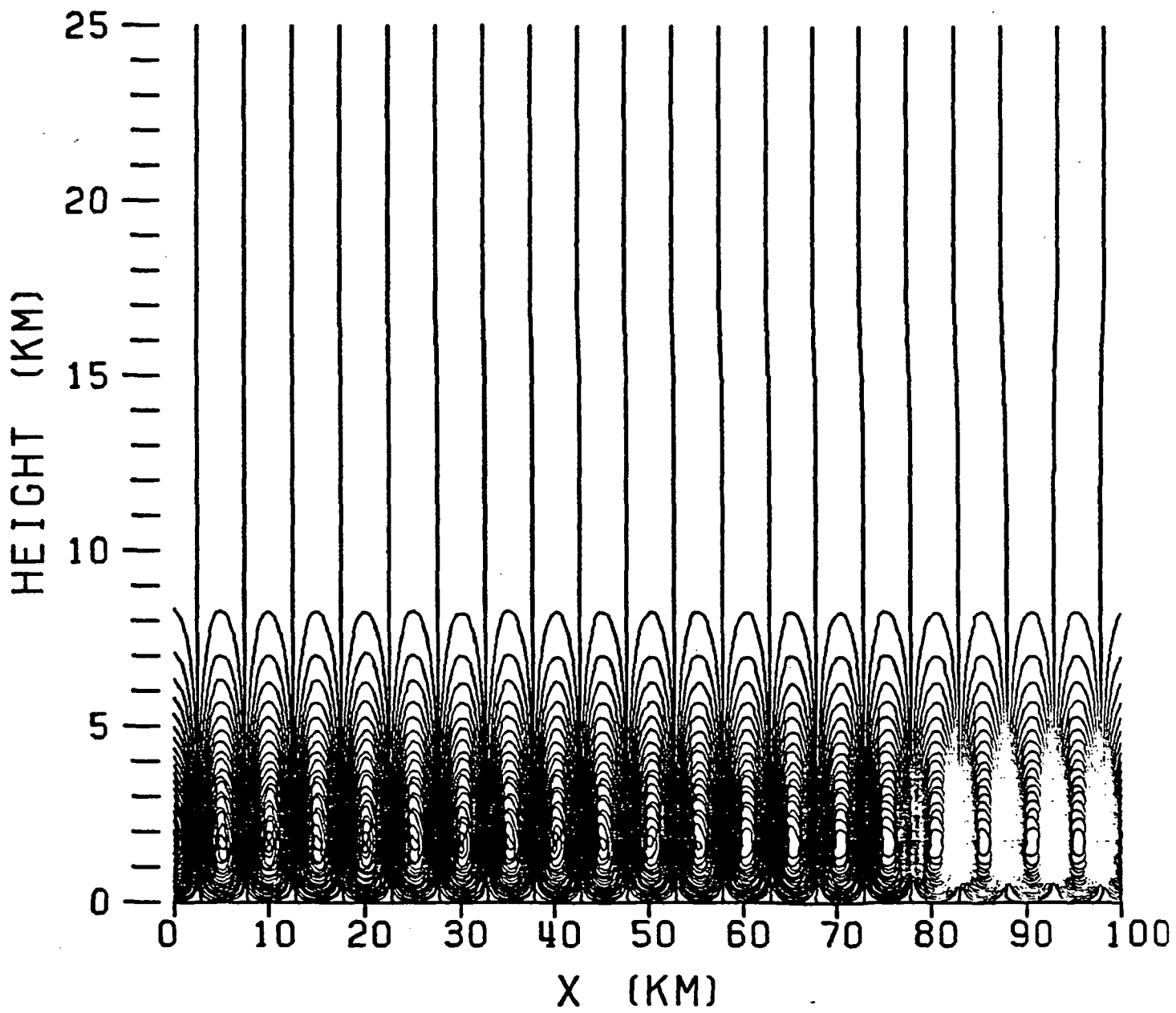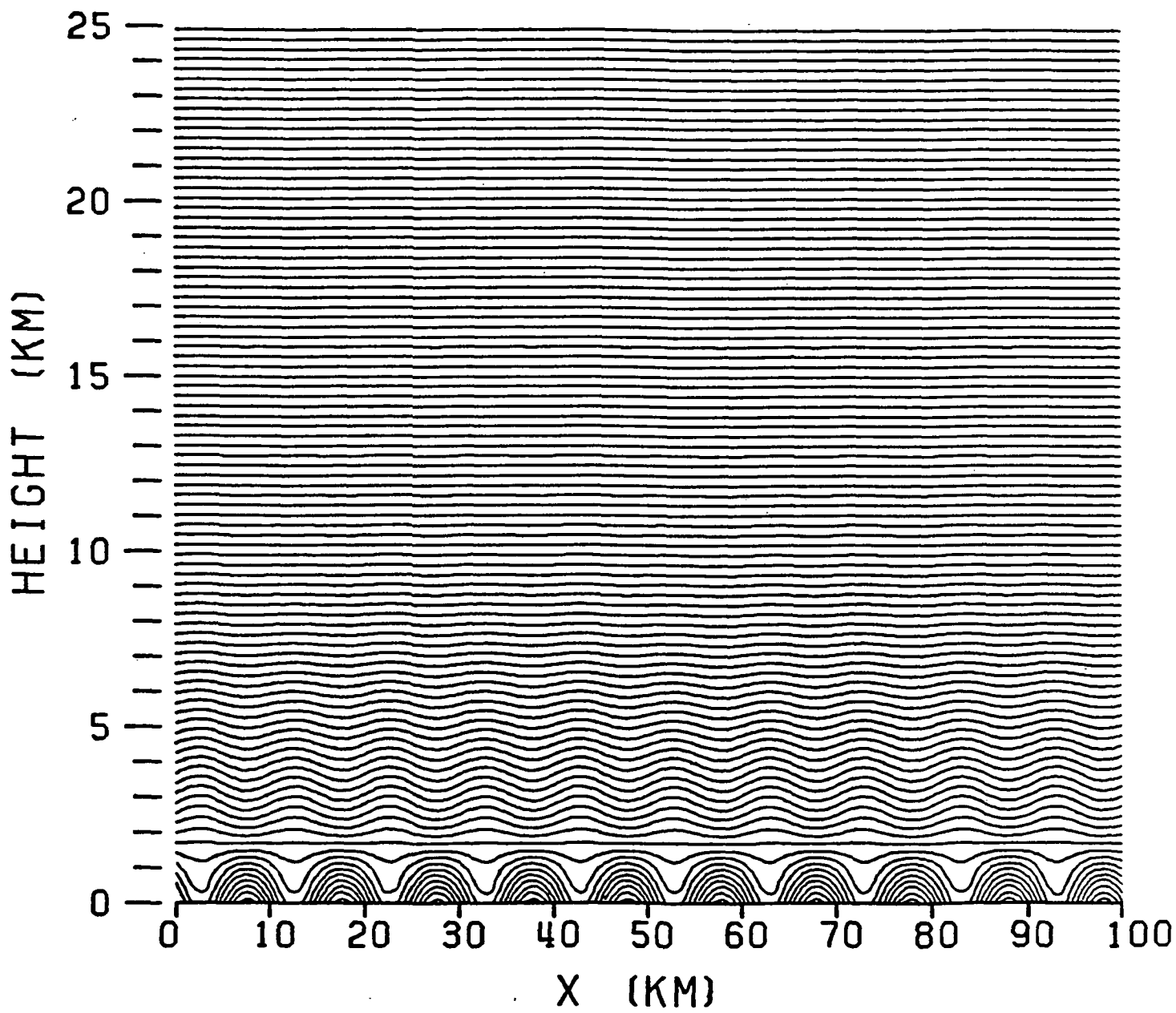SPONGE
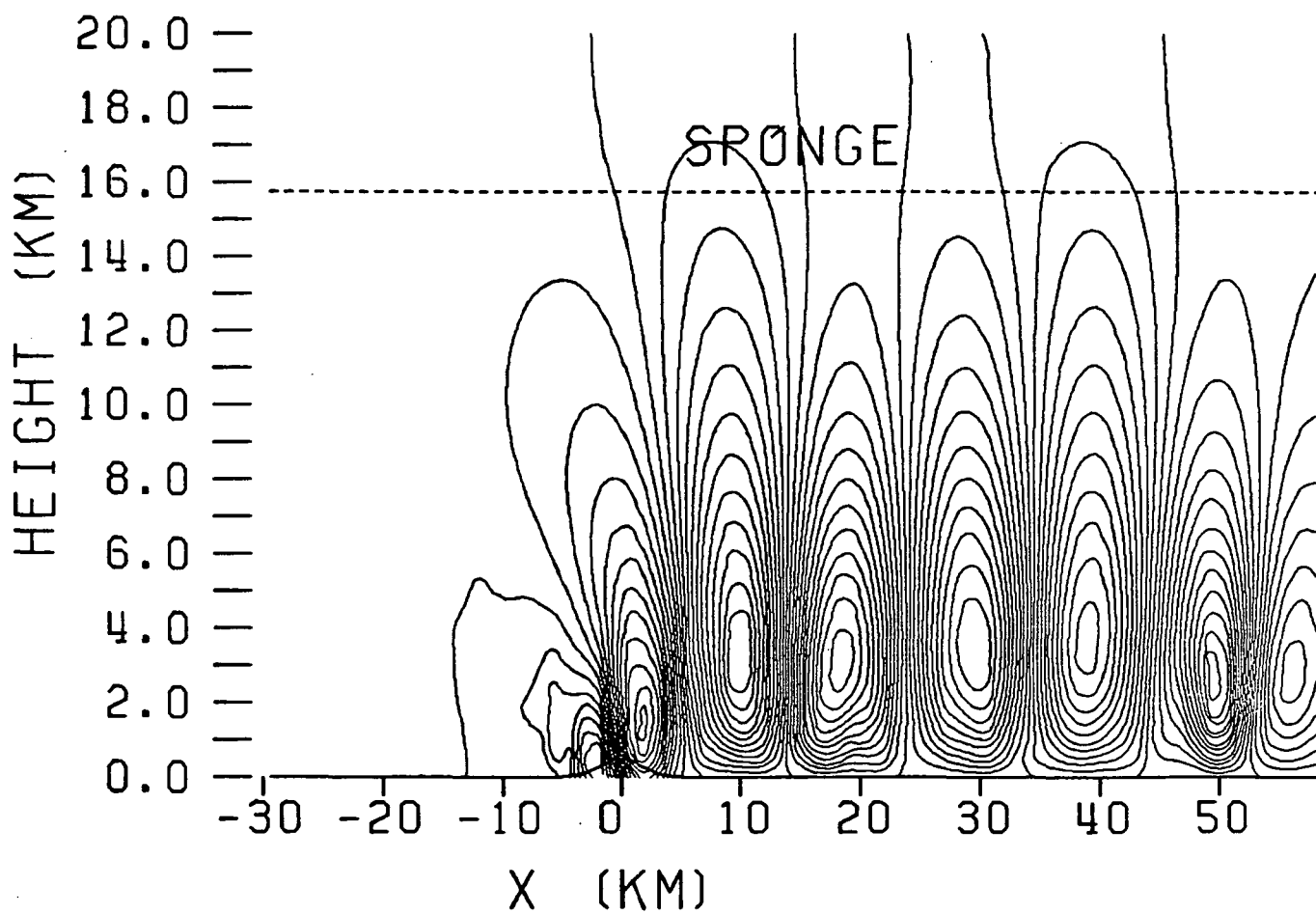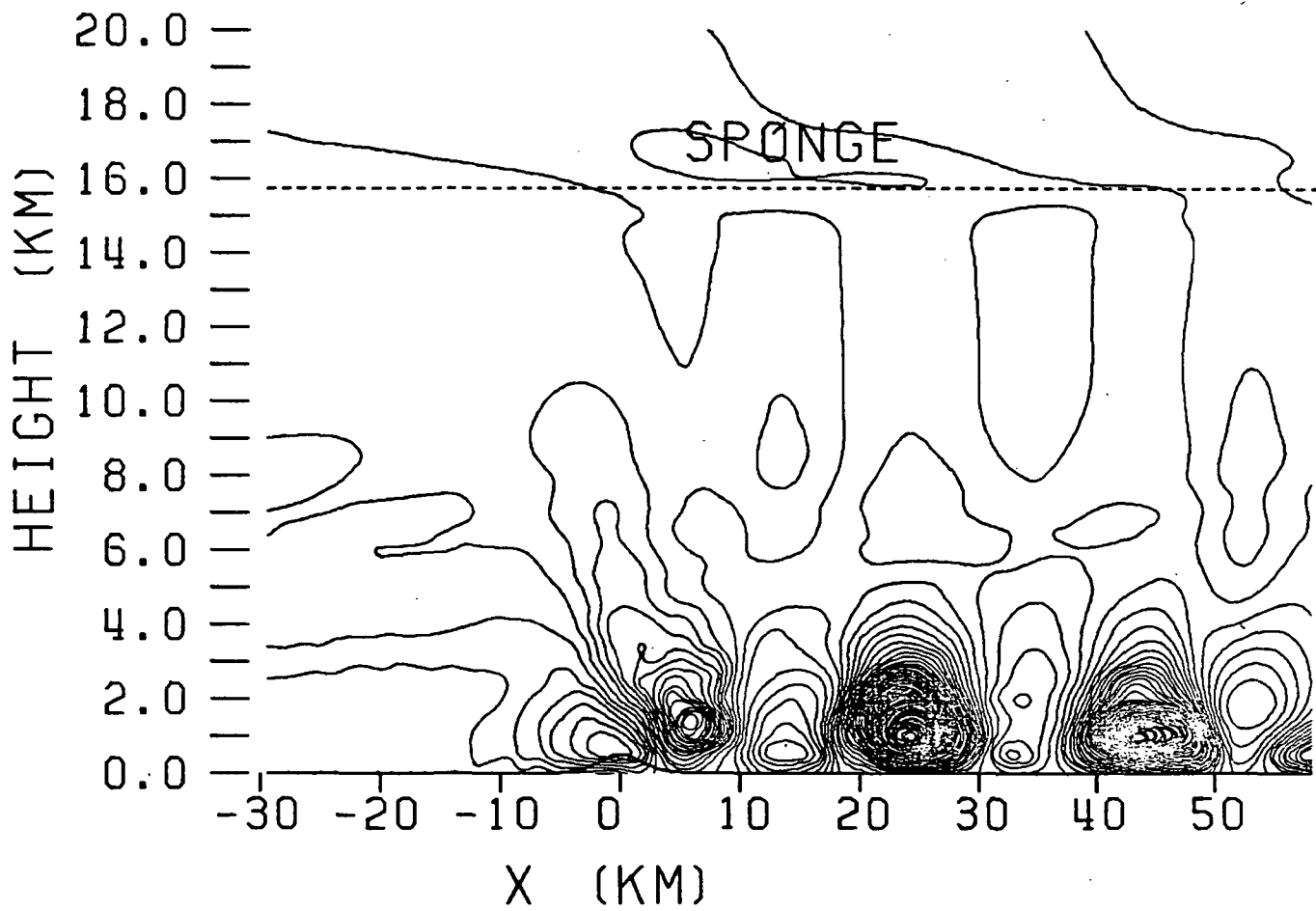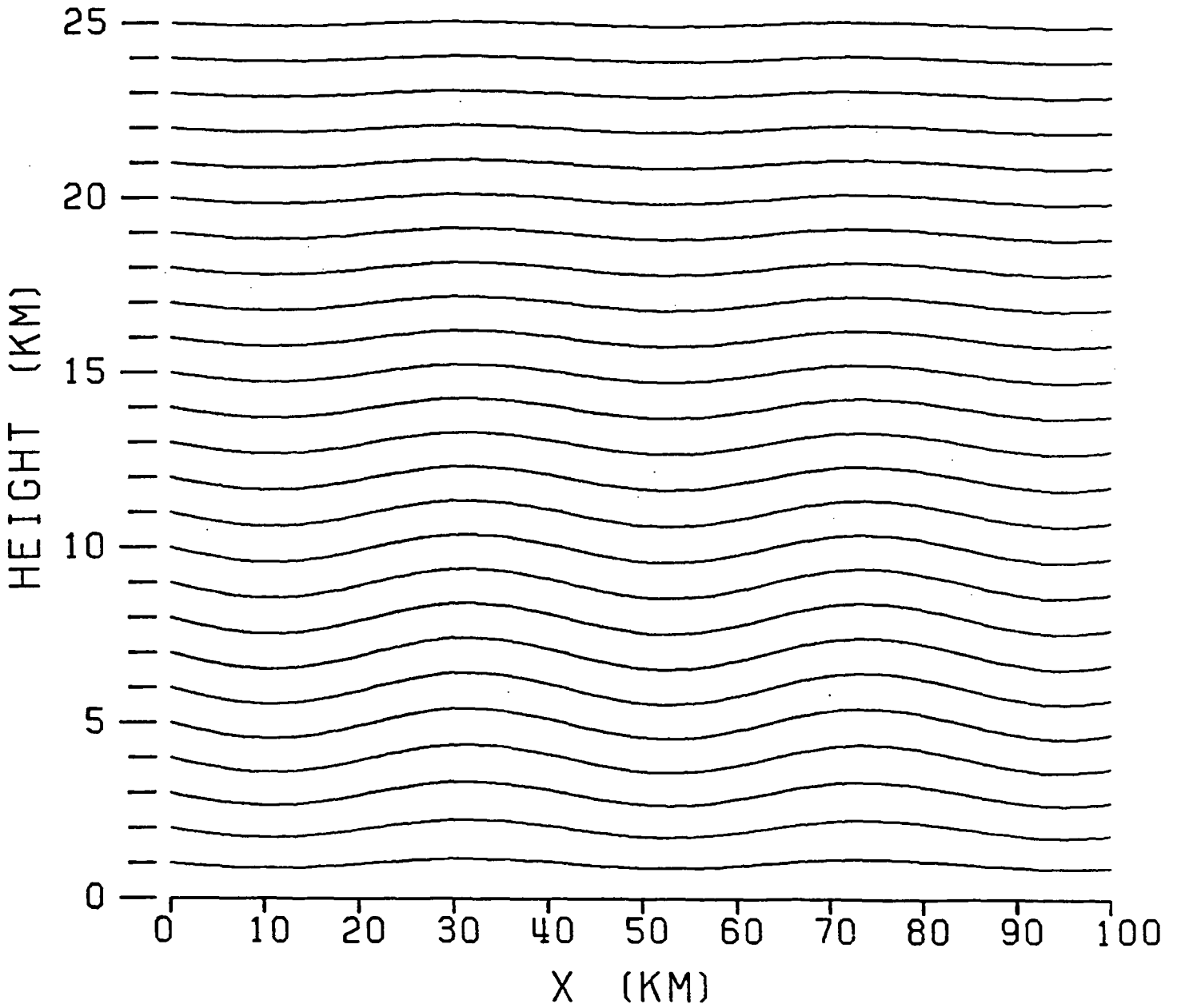
Figure 5a

Figure 5b
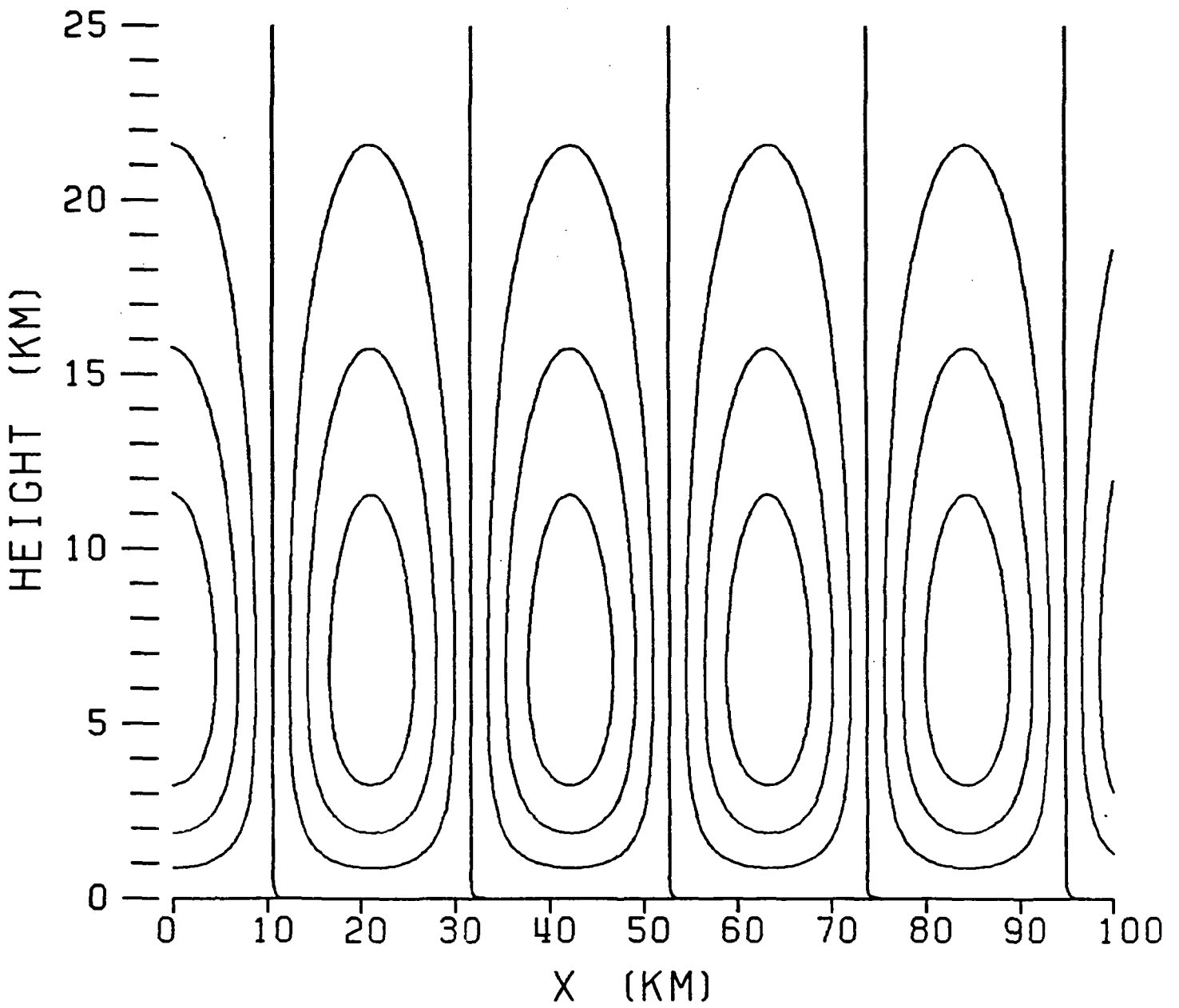
Figure 5c
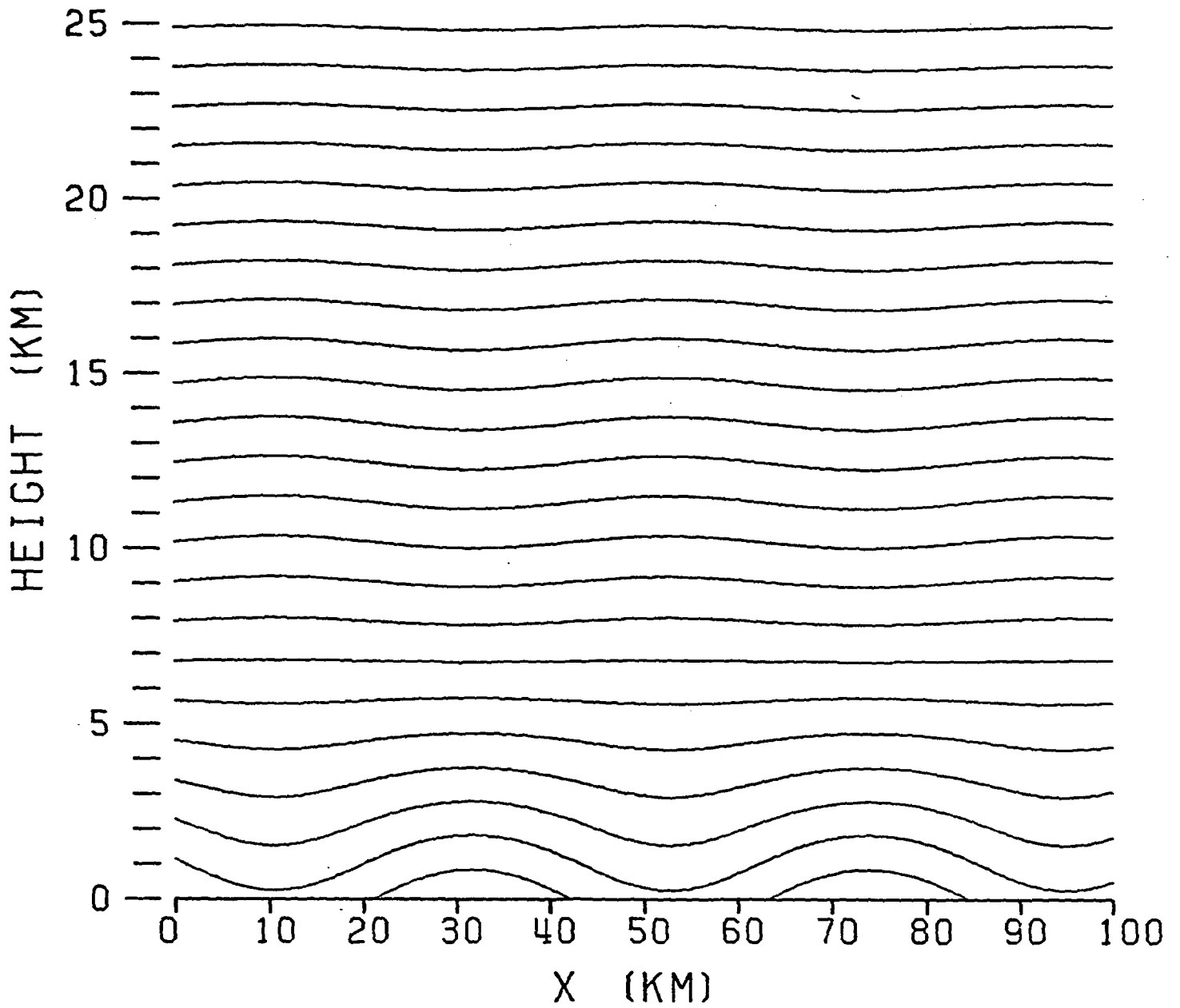
Figure 5d
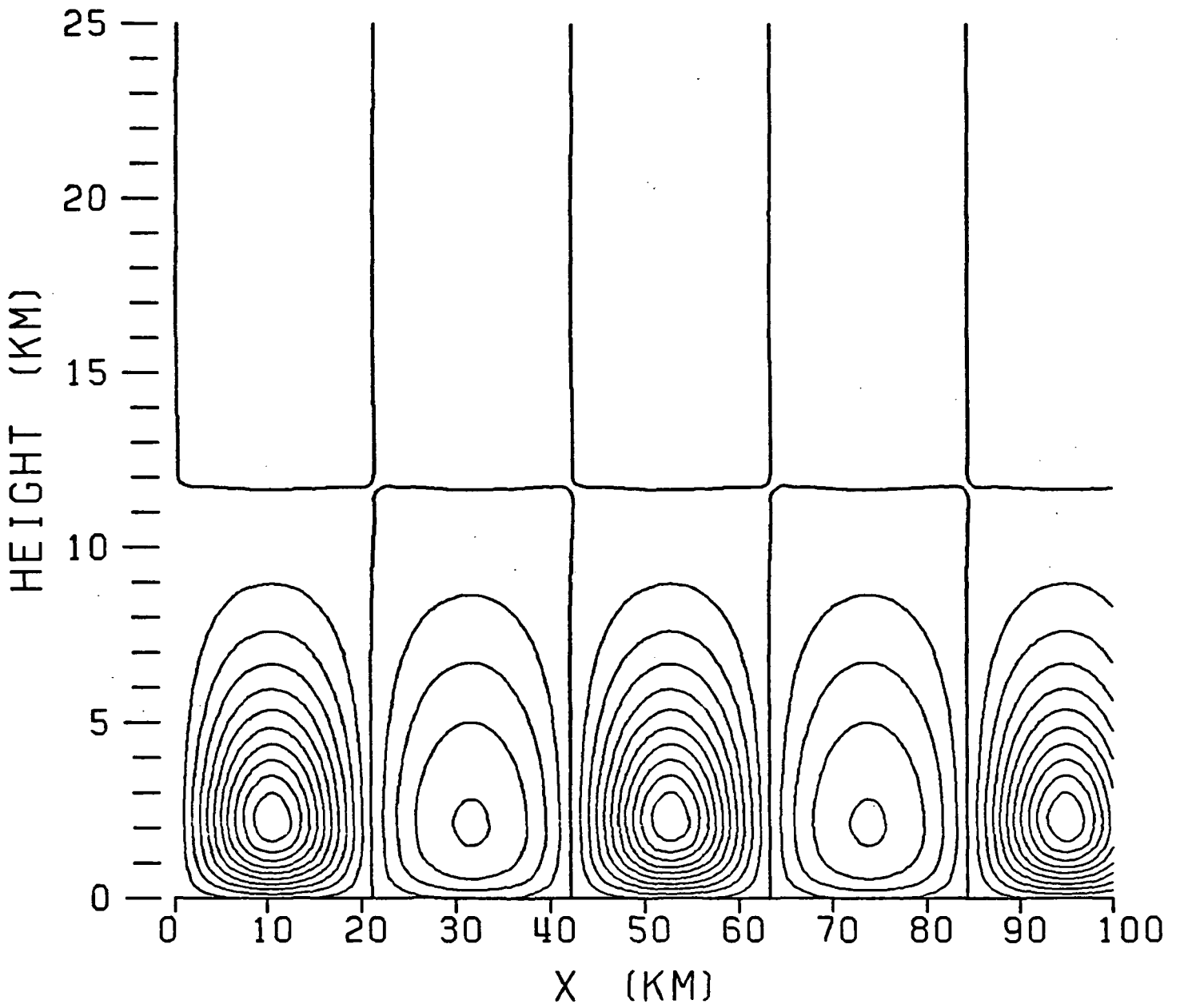
Figure 6a
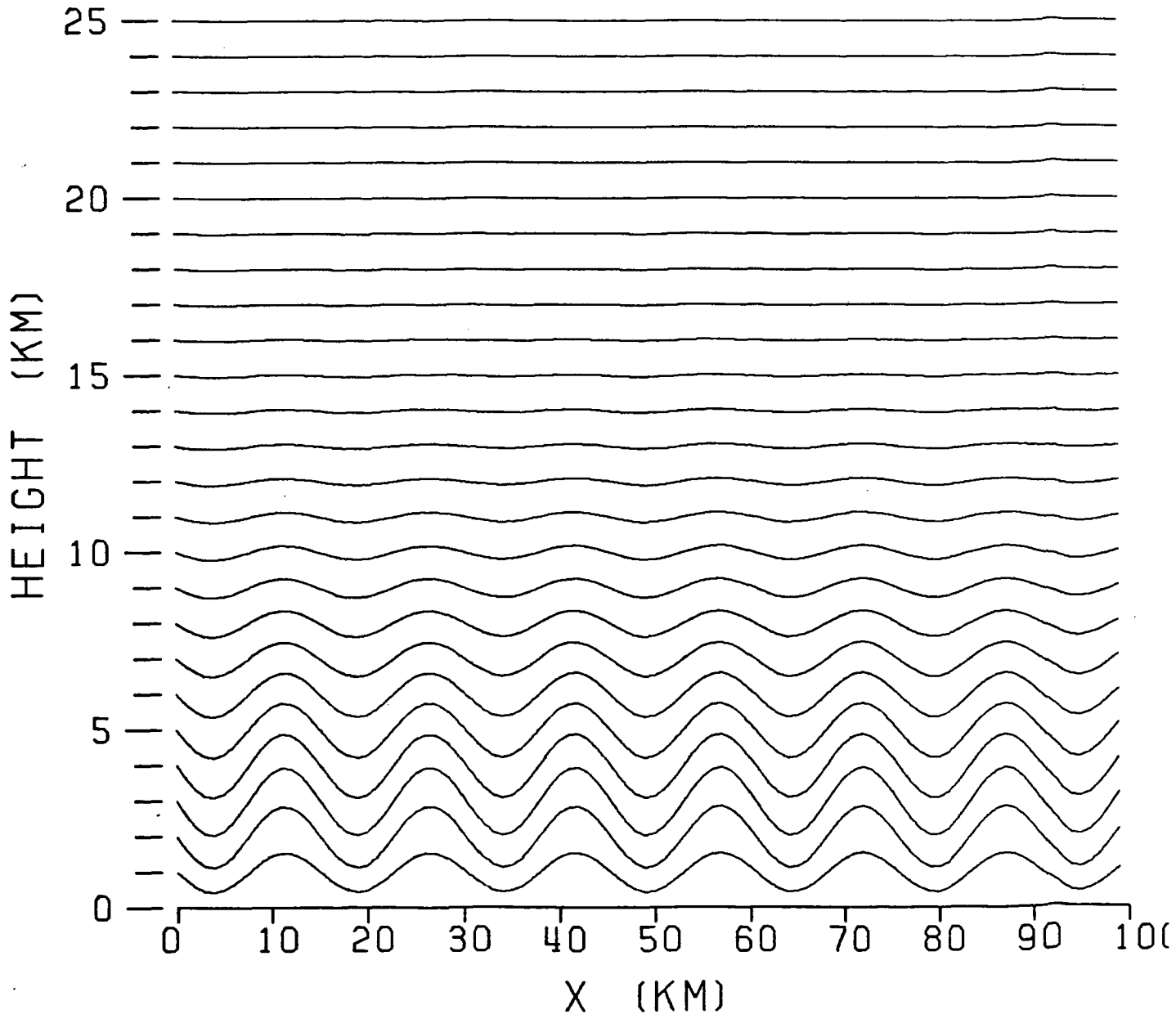
RIO = 16   MODE = 1

Figure 6b
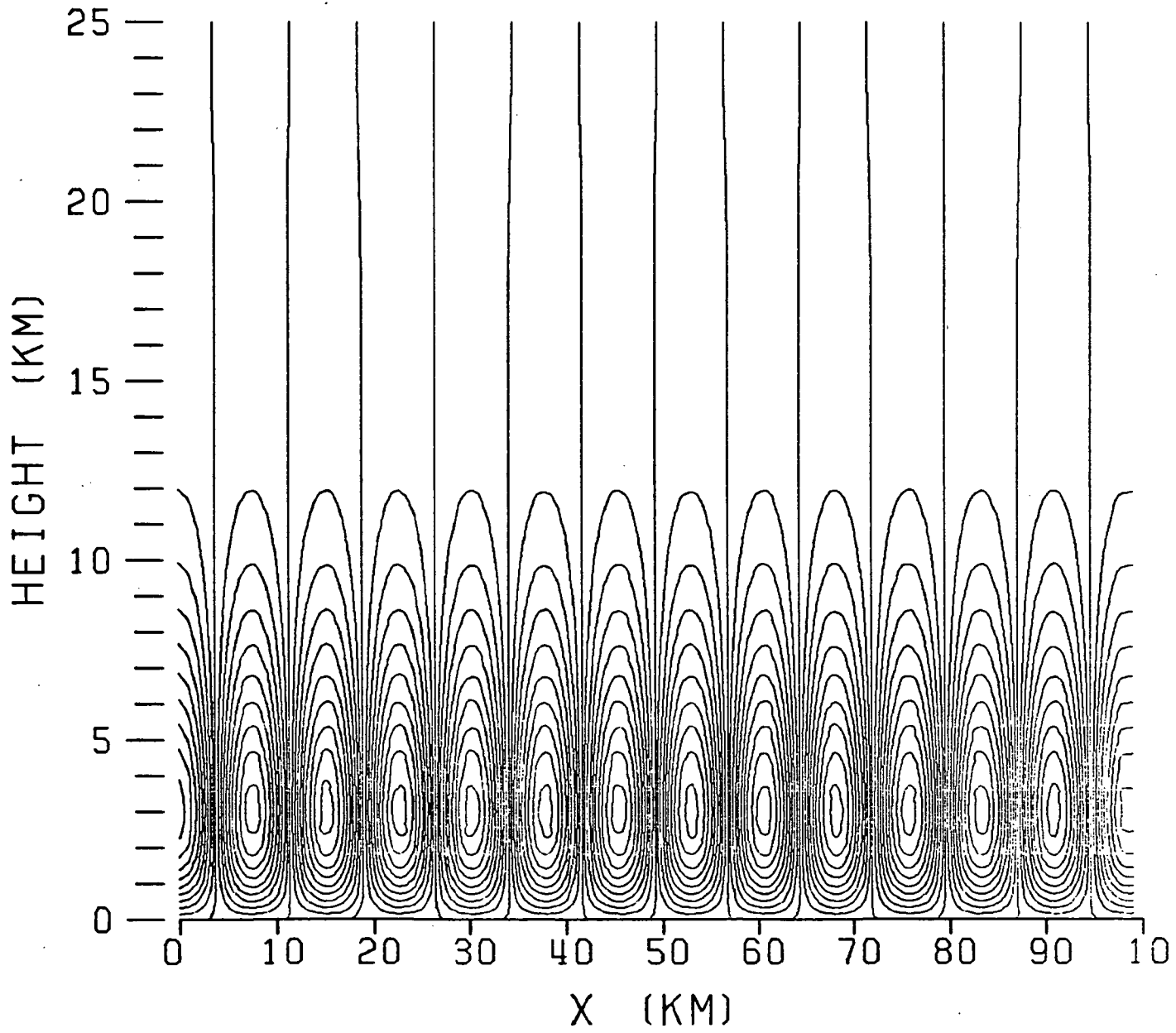
RIO = 16   MODE = 1

Figure 6c

RIO = 16   MODE = 1

Figure 6d

RIO = 16   MODE = 1

Figure 7a
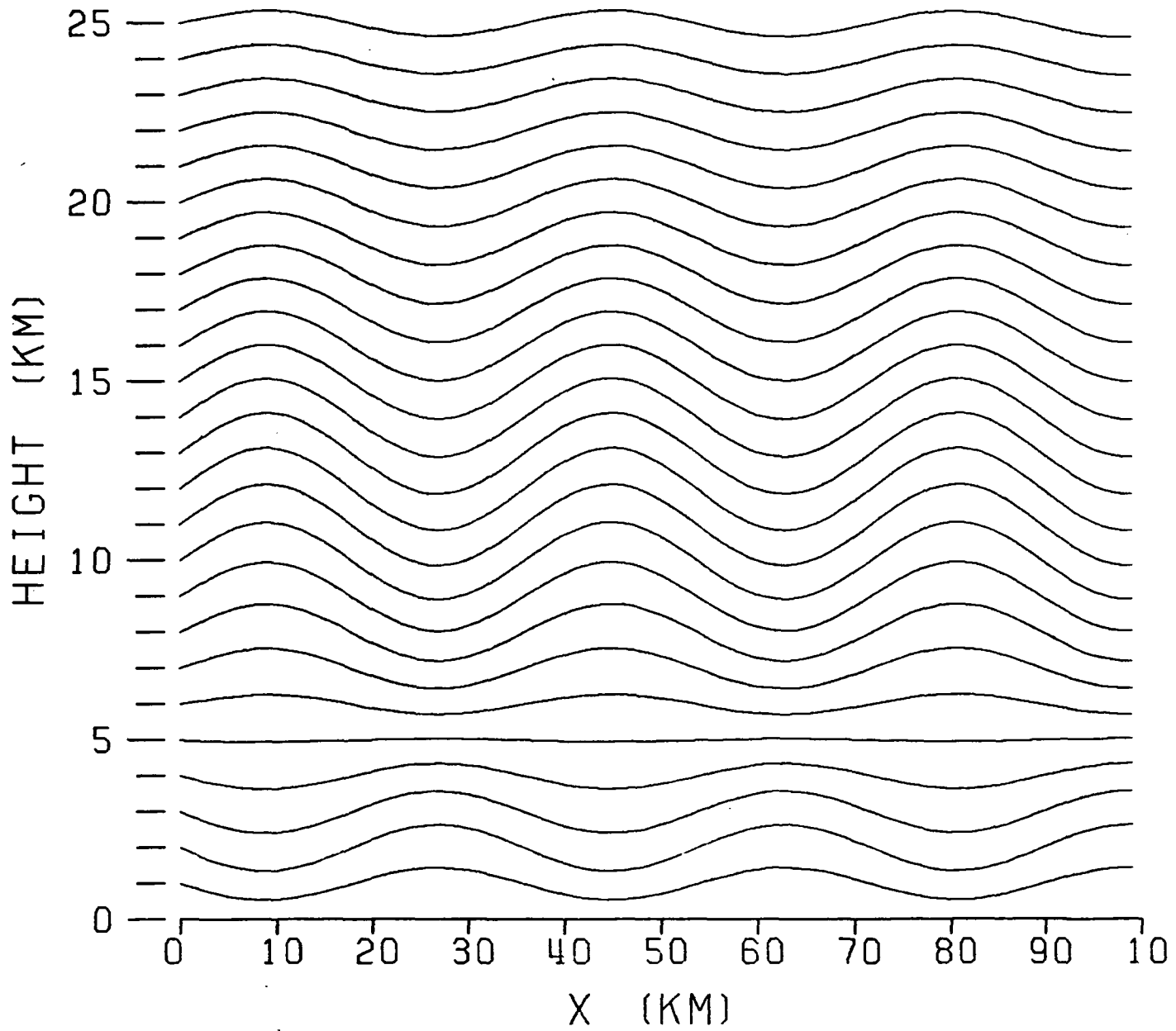
RIO = 16   MODE = 2
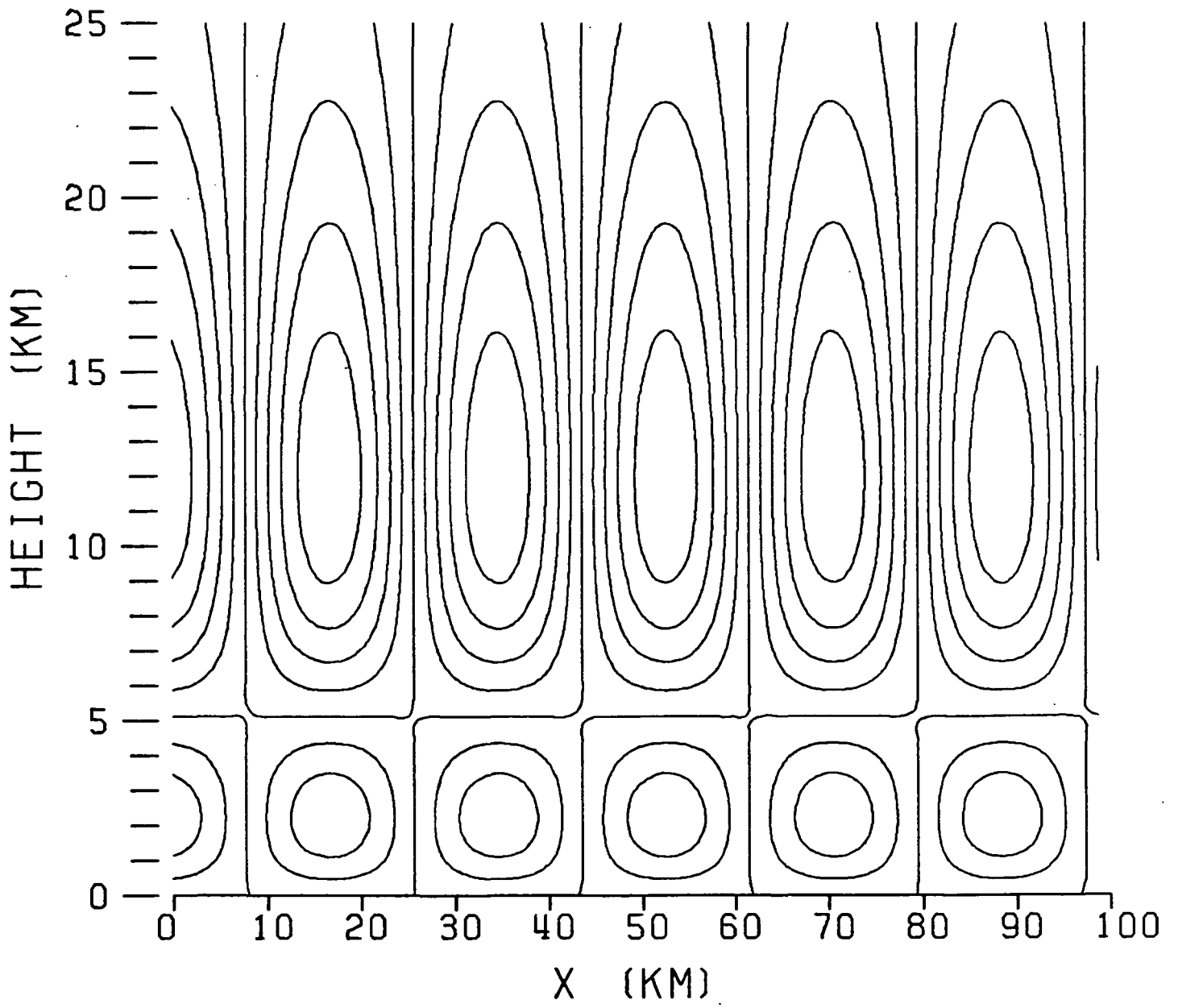
Figure 7b

RIO = 16   MODE = 2

Figure 7c
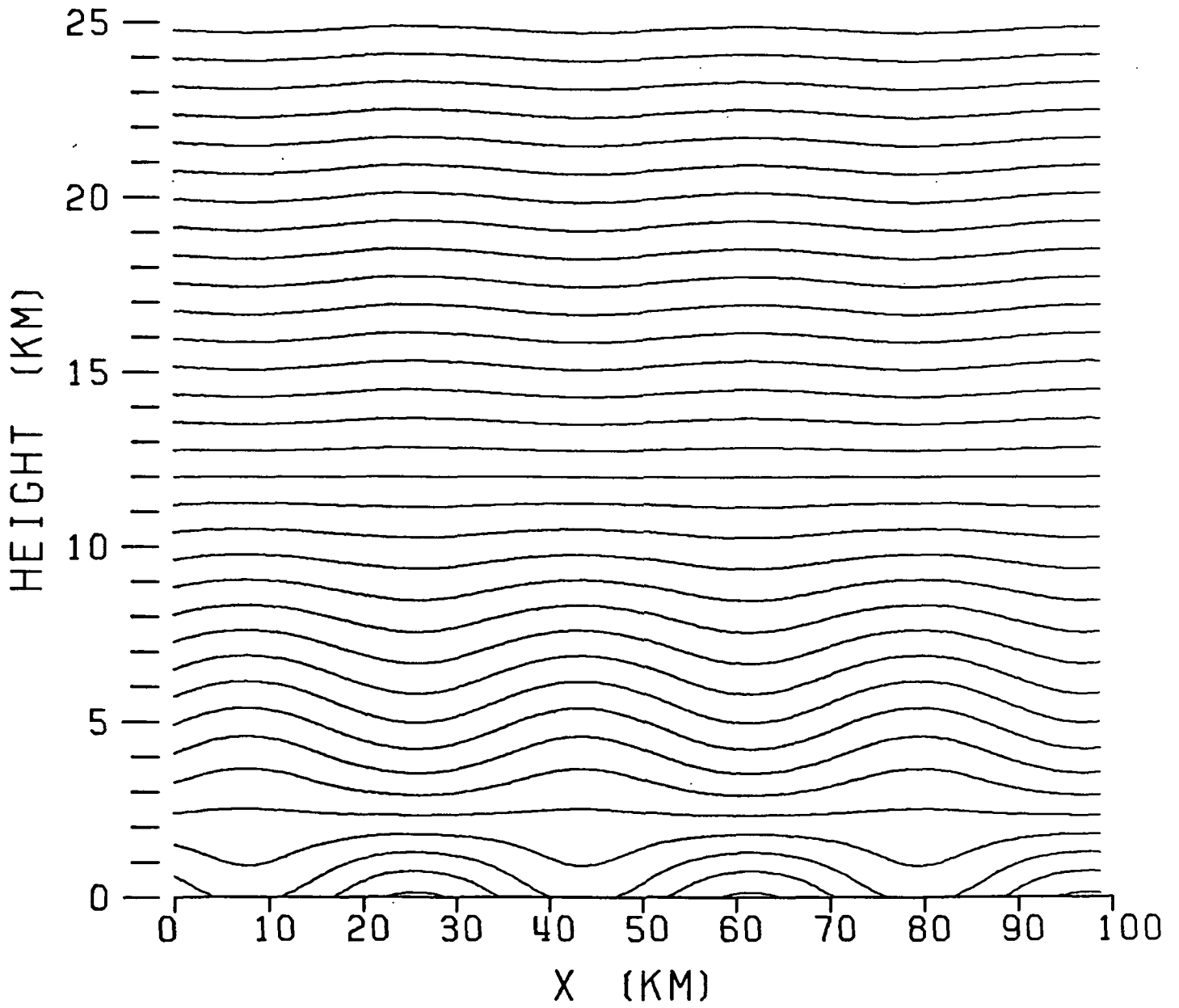
RIO = 16   MODE = 2

Figure 7d
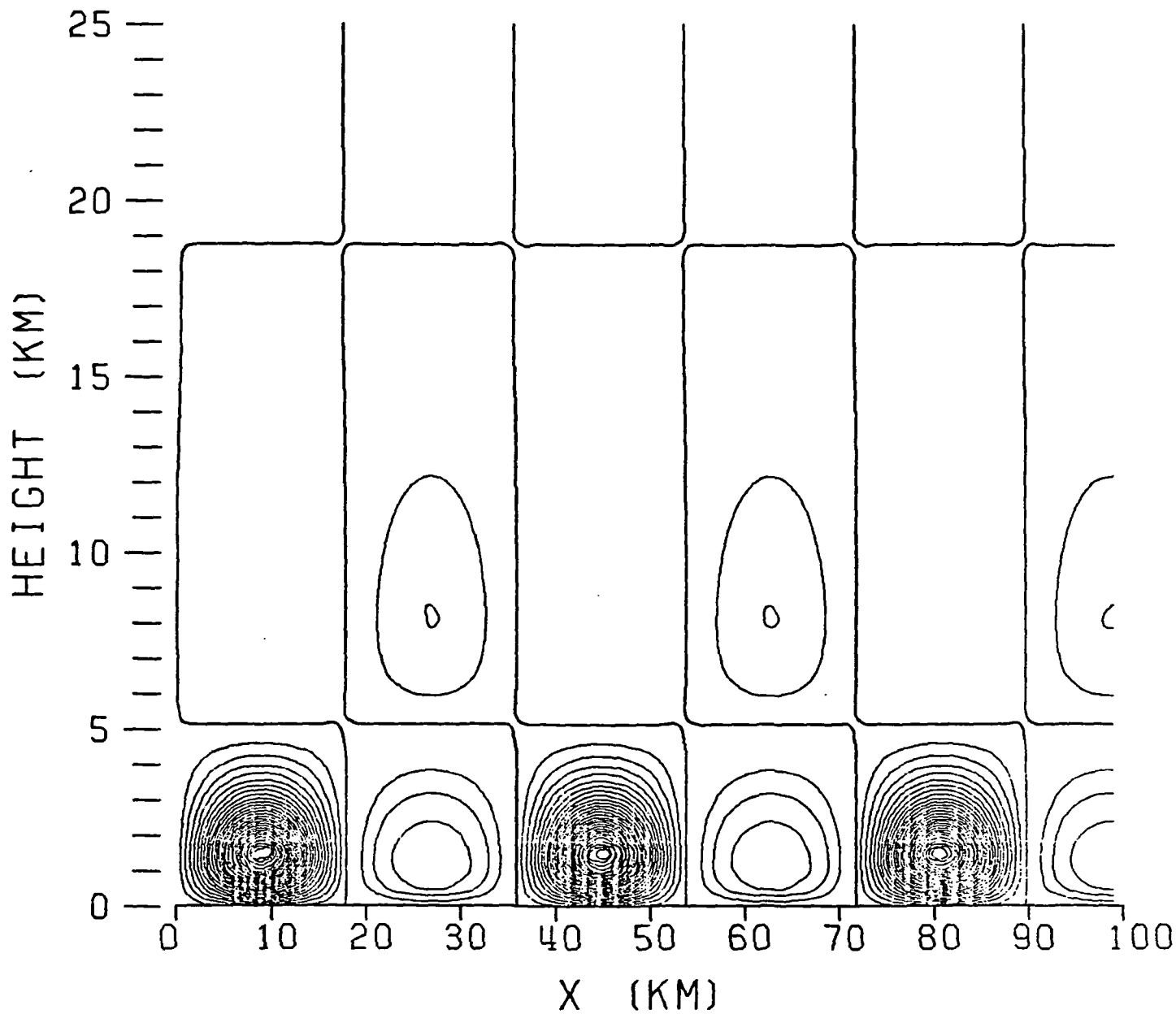
RIO = 16   MODE = 2

Figure 8a
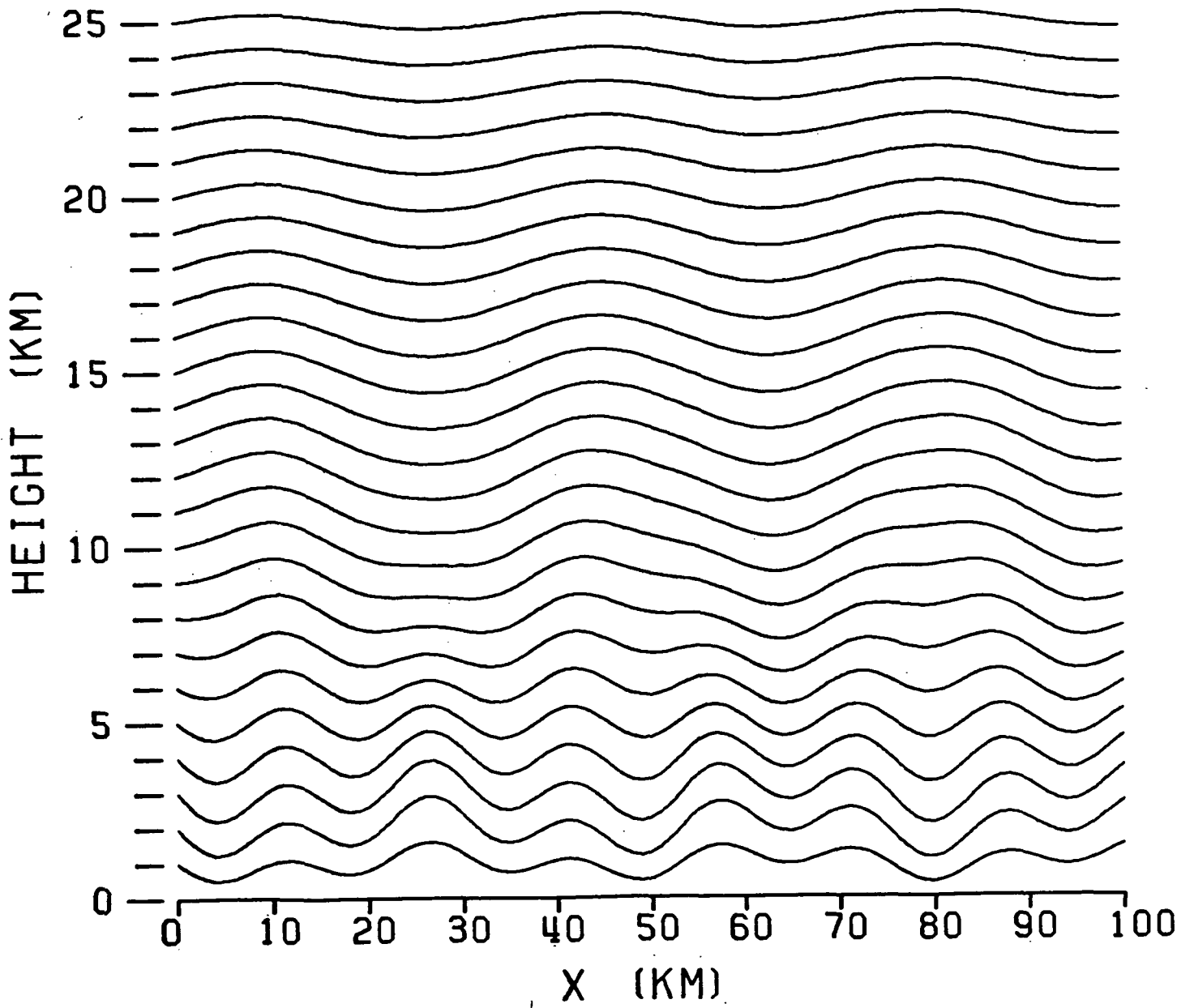
RIO = 16   2 MODE SUM

Figure 8b
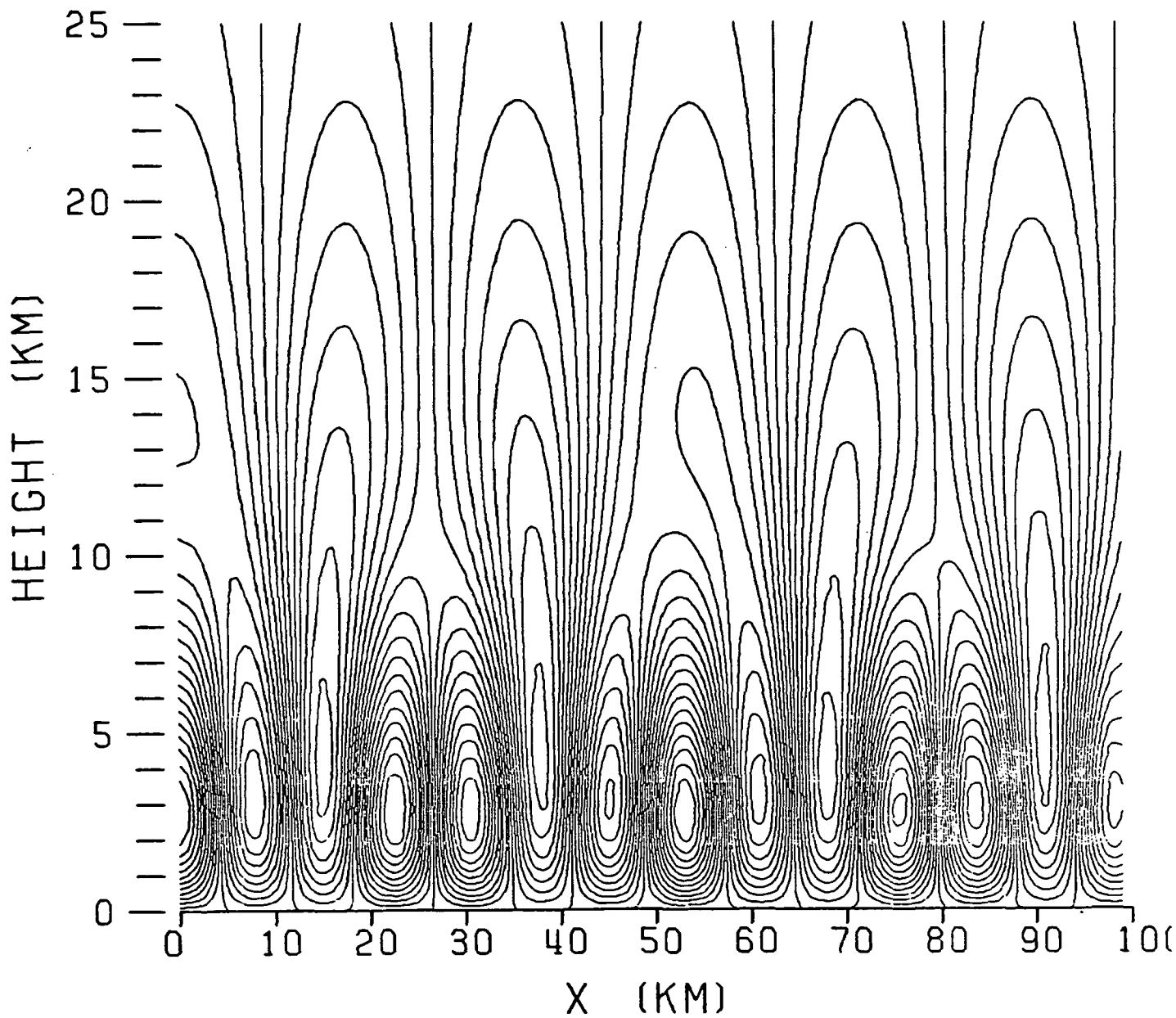
RIO = 16   2 MODE SUM

Figure 8c
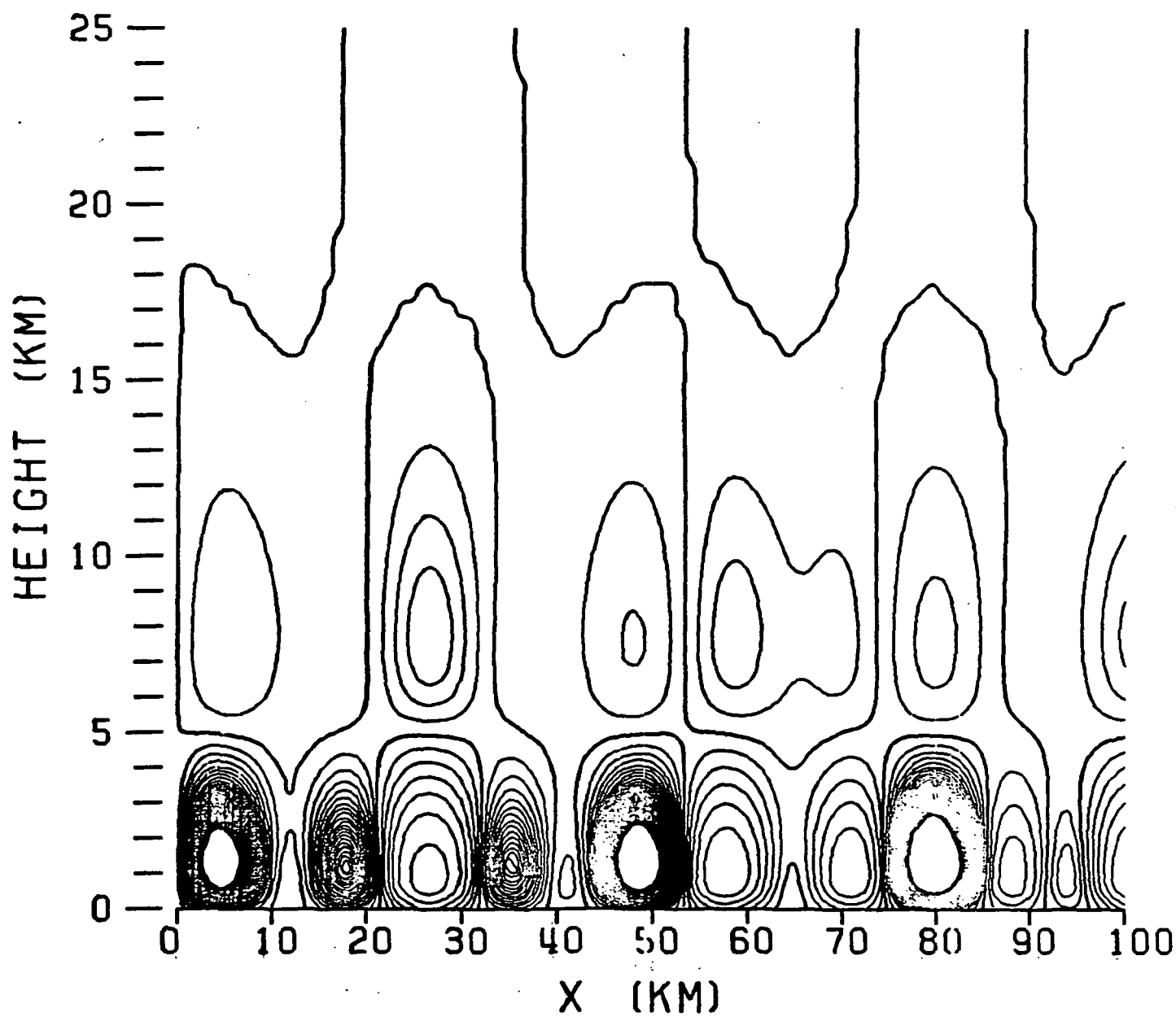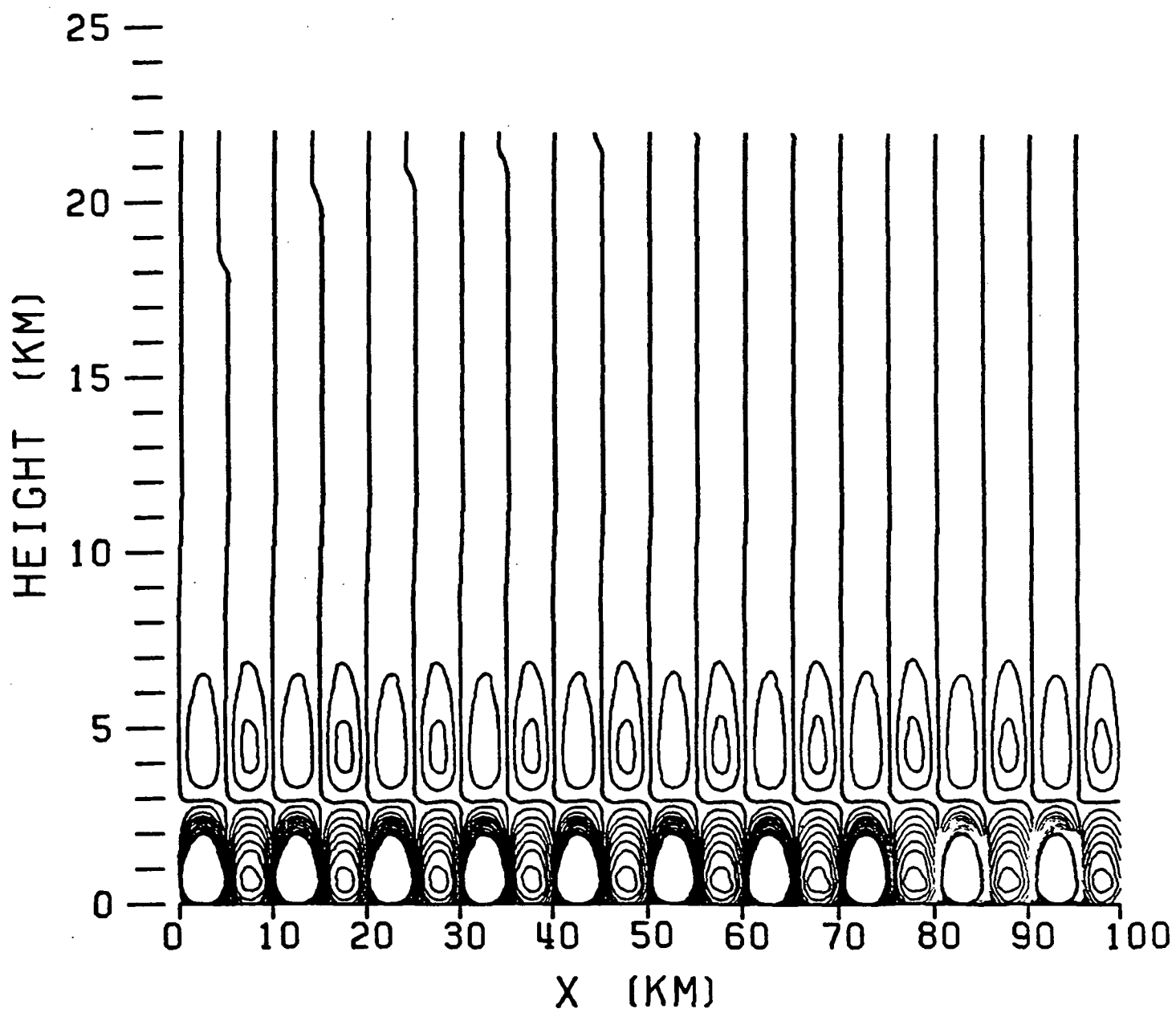

RIO = 16   2 MODE SUM
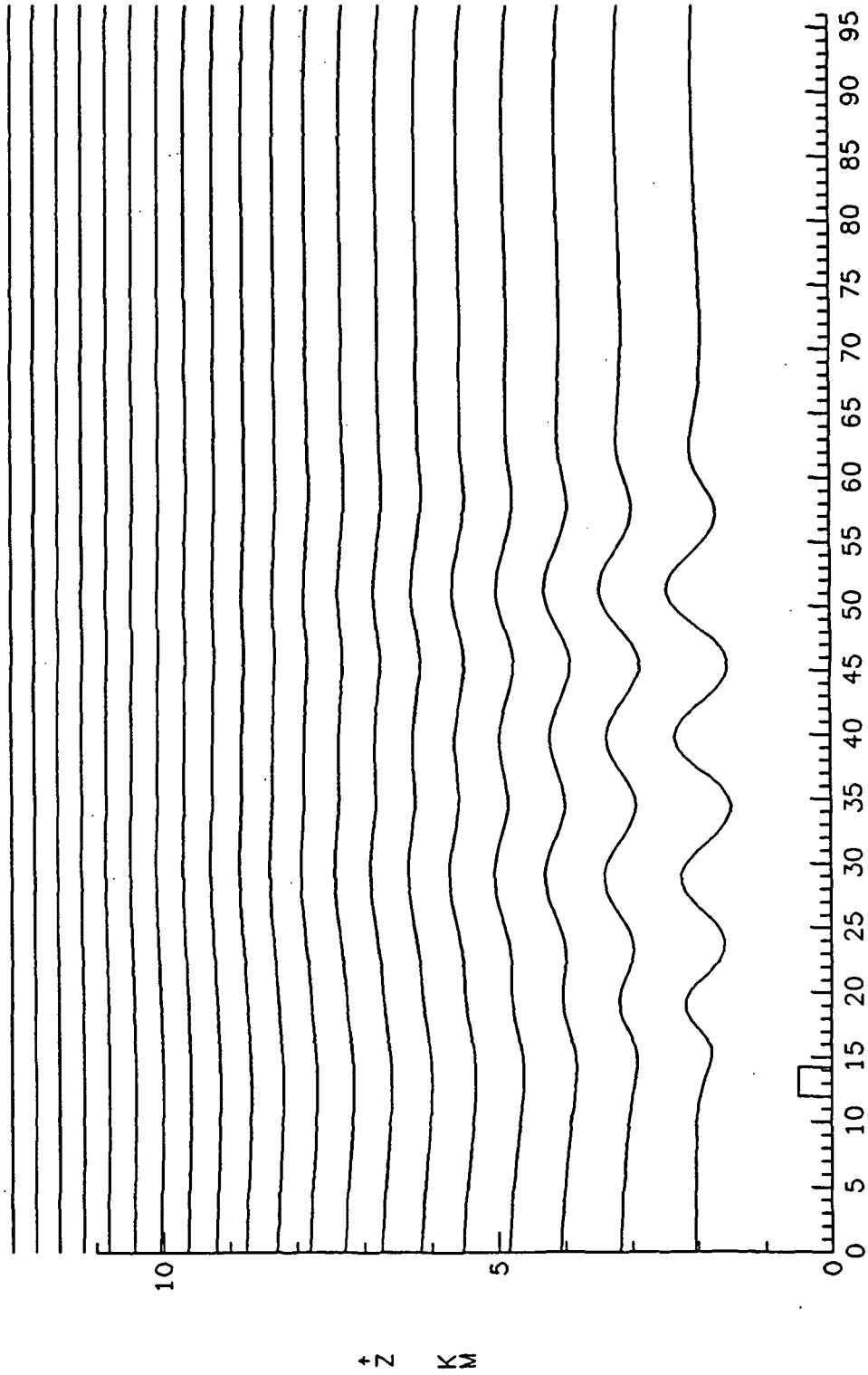
Figure 9a

Figure 9b

Figure 9c

Figure 9d

Figure 10a

Figure 10b
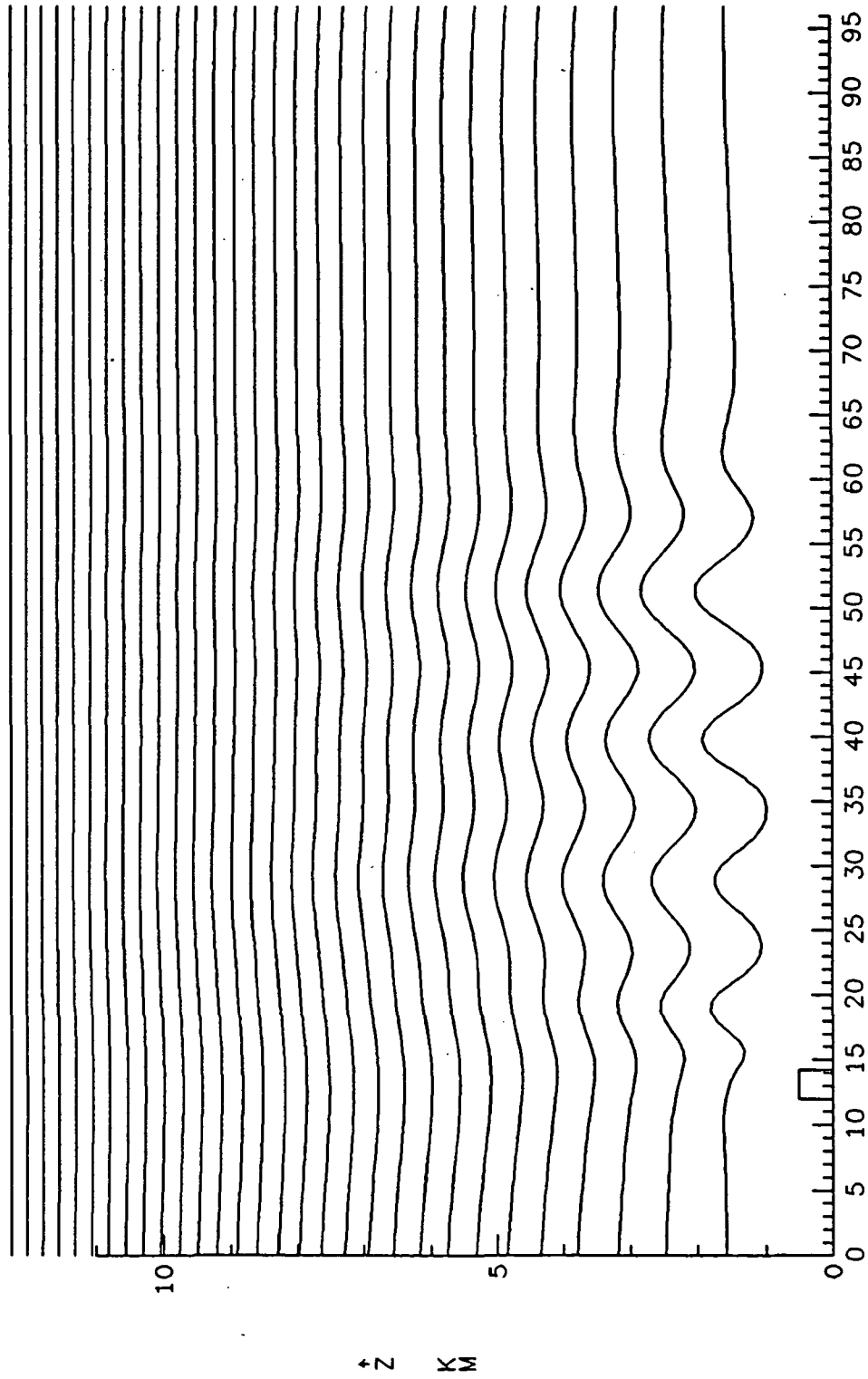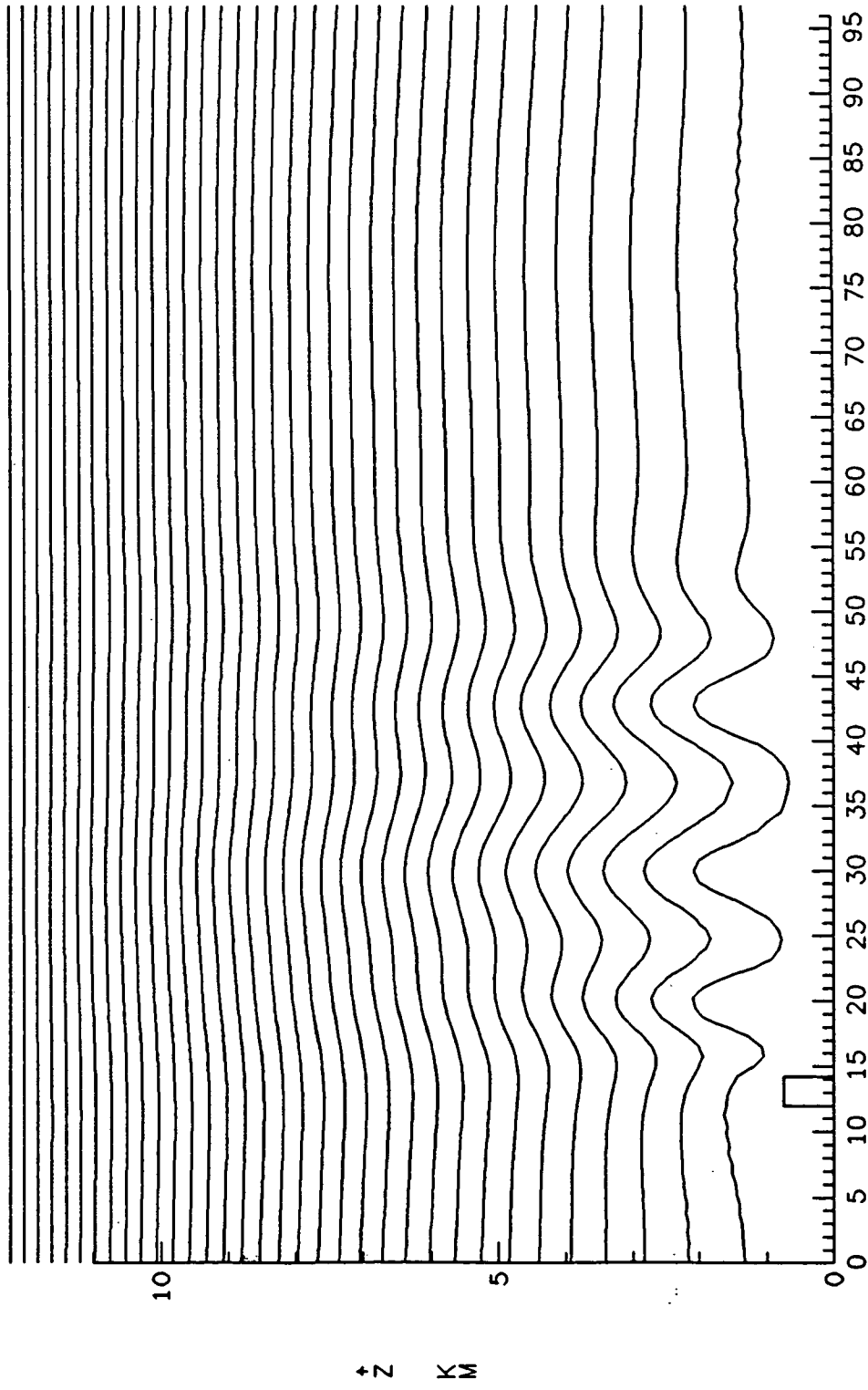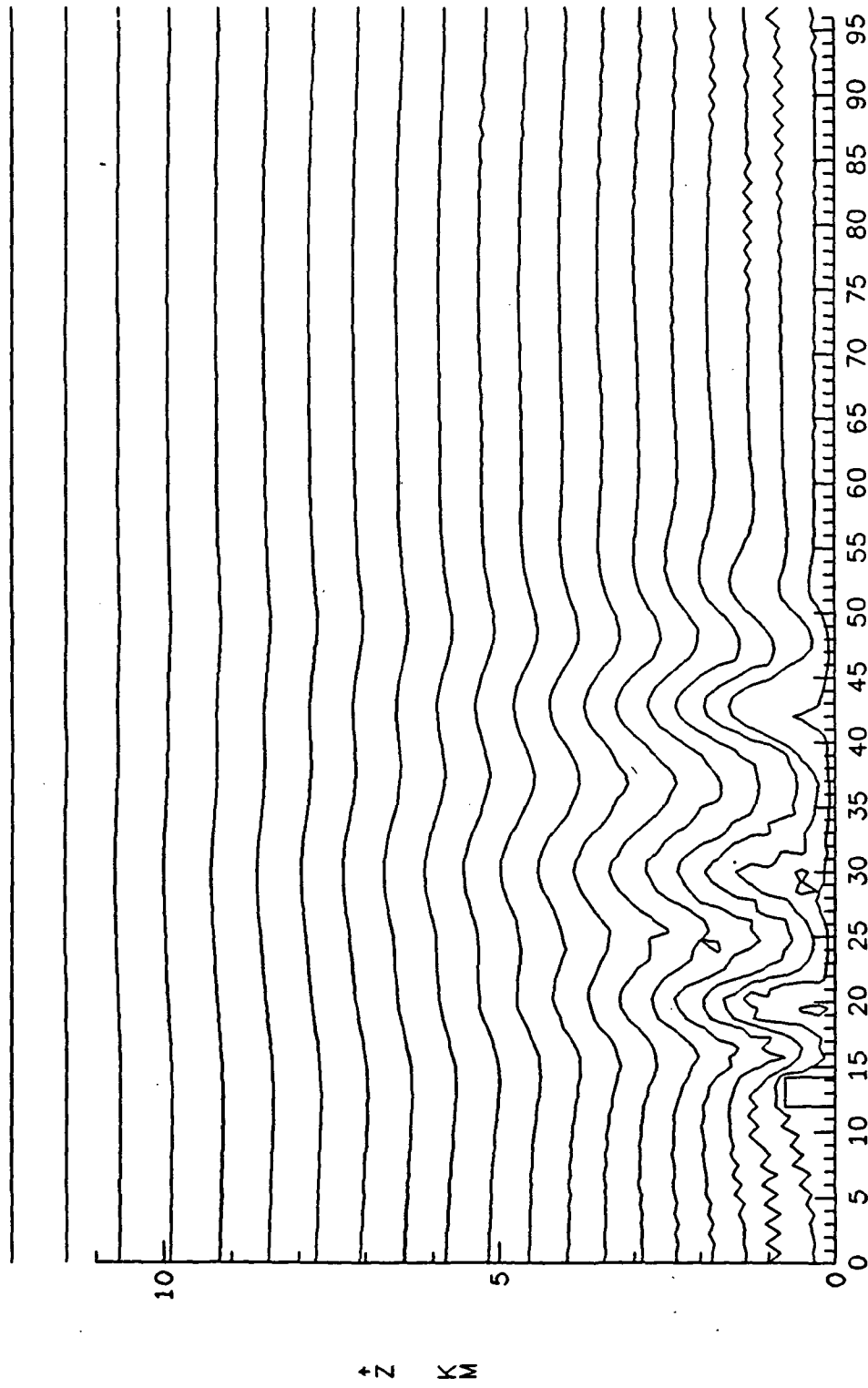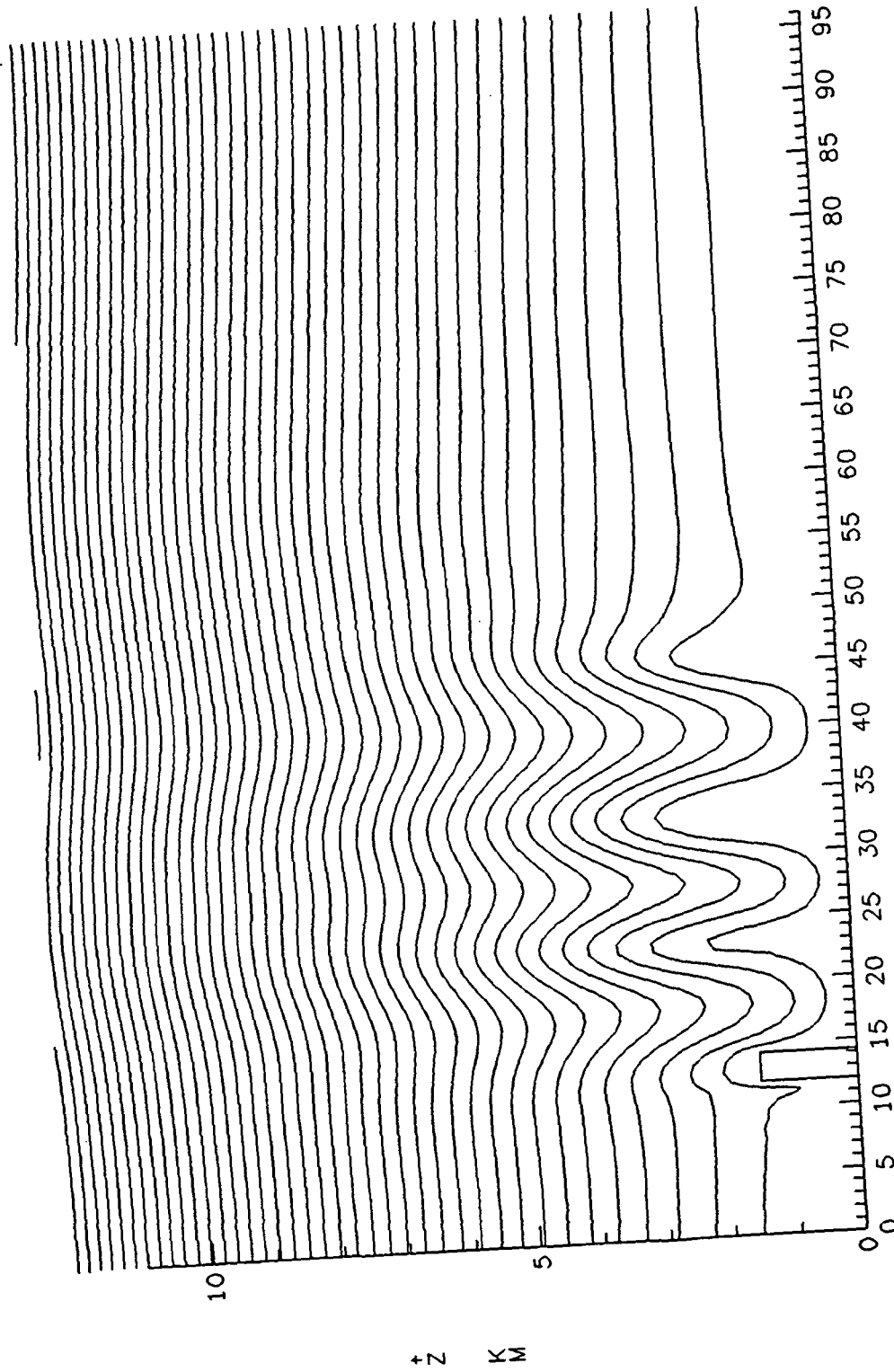
Figure 11a
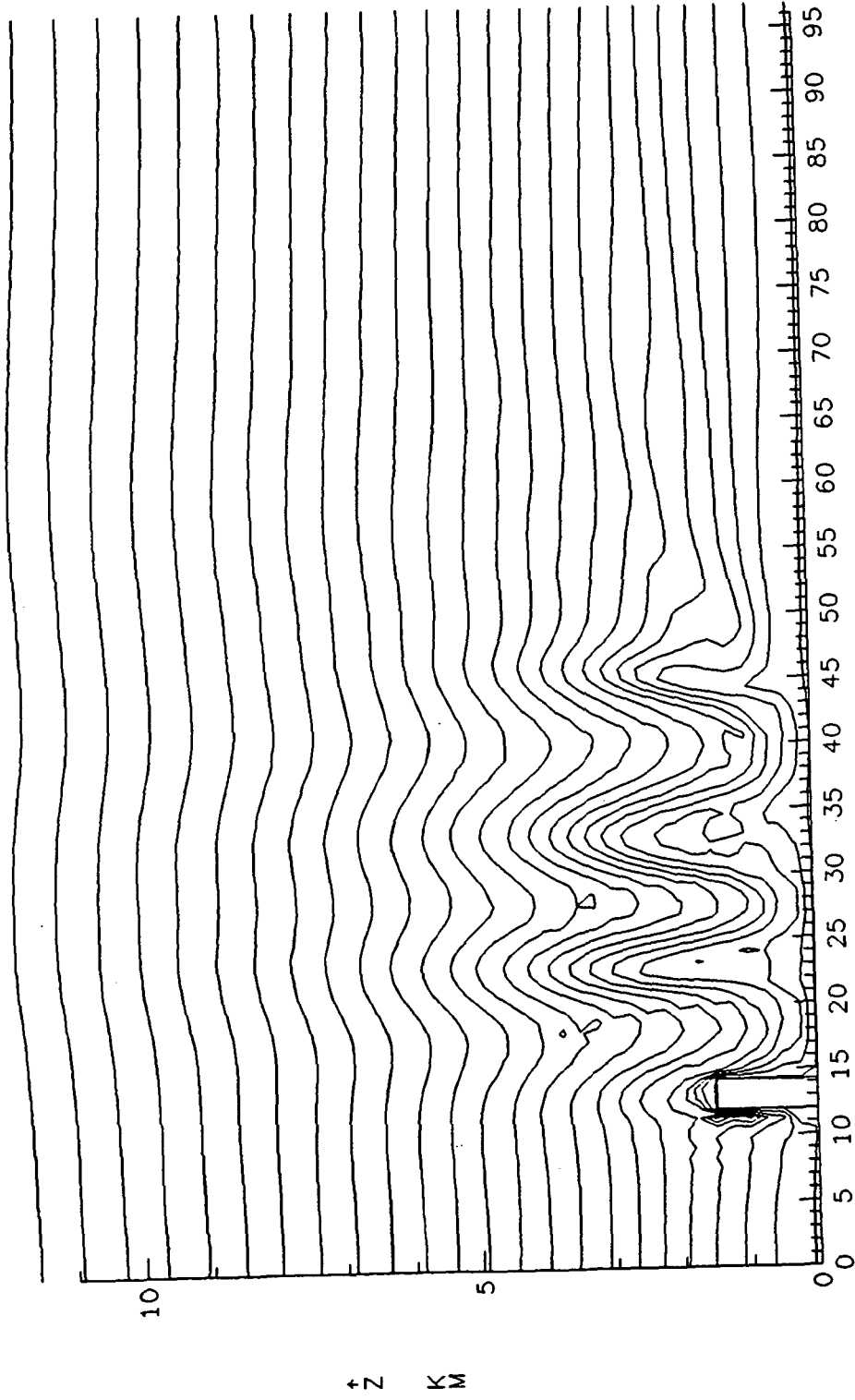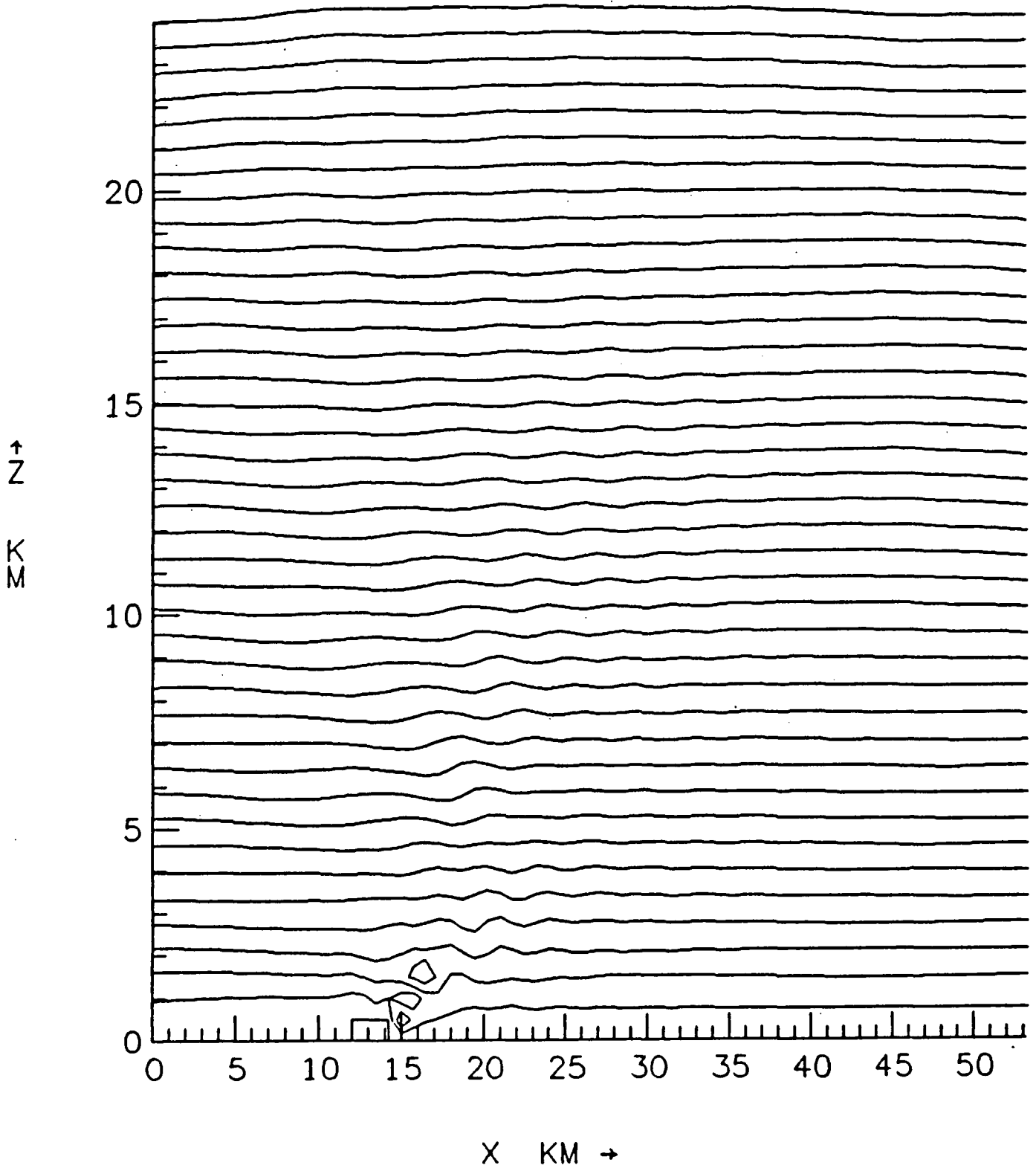
Figure 11b

Figure 12a

-65-

Figure 12b

Figure 13

APPENDIX A

The modified Bessel function $K_\nu(\xi)$ is discussed and tabulated for real ν and ξ in may sources (e.g. Abramowitz and Stegun, 1964; Sections 9.6-9.8). However, the useful function $K_{i\mu}(\xi)$, although arising naturally in fluid dynamical contexts (e.g. Booker and Bretherton, 1967; Mowbray and Rarity, 1967) seems to have been tabulated only by Morgan (1947). Morgan's work is relatively difficult of access; and since it was done at a time when computing capability was relatively slight, his tables provide less than adequate resolution. Therefore, we present here some relevant formulas and a diagram illustrating the behavior of the function.

A qualitiative characterisation is easily obtained by means of the integral representation

$$K_{i\mu}(\xi) = \int_0^\infty \cos(\mu t)\, \exp(-\xi \cosh t)\, dt \tag{A1}$$

derived from Abramowitz and Stegun (1964, 9.6.24) by the substitution $\nu = i\mu$. From this formulation, by straightforward application of the method of steepest descents, we derive the following two asymptotic limits, for $\mu \gg \xi$ and $\mu \ll \xi$. For $\mu \gg \xi$,

$$K_{i\mu}(\xi) \sim \left(\frac{2\pi}{\mu}\right)^{1/2} \exp\left(-\mu\frac{\pi}{2}\right) \sin\left[\mu\left(\ln\mu - \ln\frac{\xi}{2} - 1\right) + \frac{\pi}{4}\right] \tag{A2}$$

and for $\mu \ll \xi$

$$K_{i\mu}(\xi) \sim \left(\frac{\pi}{2\xi}\right)^{1/2} e^{-\xi} \tag{A3}$$

These are given by Morgan (1947). Thus in the range $\mu \sim \xi$, $K_{i\mu}(\xi)$ changes from oscillatory to exponential behavior as ξ increases. The oscillatory singularity in (A2) for $\xi \to 0$ is familiar as arising in the problem of the propagation of a gravity wave toward a critical level.(Booker and Bretherton, 1967).

The values of $K_{i\mu}(\xi)$ for use in Section 2 were calculated using three different relations for various ranges of the parameters μ and ξ . For large ξ ($|\xi| > 20$, or $|\xi| > 5$ and $2|\xi| > \mu^2$, or $|\frac{\xi^2}{4}| > 5\mu$), the asymptotic relation (A3) with higher order terms included (see e.g. Abramowitz and Stegun Eq. 9.7.2) was used. For large μ ($\xi > 20$, $\mu > \xi$) Debye's asymptotic expansion (A2) with higher order terms included (see Abramowitz and Stegun Eq. 9.3.7) gave satisfactory results. For all other parameter values the standard ascending series (Abramowitz and Stegun Eq 9.1.10) was used to compute $J_{i\mu}(i\xi)$, with the value of $K_{i\mu}(\xi)$ provided by the identity

$$K_{i\mu}(\xi) = -\frac{\pi}{\sinh(\mu\pi)} \, \Im m \left\{ \exp\left(\frac{\mu\pi}{2}\right) J_{i\mu}(i\xi) \right\}$$

The leading term of the result of this process reduces to

$$K_{i\mu}(\xi) \doteq \left(\frac{\pi}{\mu \sinh \mu\pi}\right) \cos\left[\mu \ln \frac{\xi}{2} - \arg \Gamma(i\mu)\right]$$

where Γ represents the gamma function. This representation is also given in Morgan (1947).

The most convenient form for visual representation of the function $K_{i\mu}(\xi)$ is a contour plot in (μ,ξ)-space, following Jahnke, Emde, and Losch (1960, Figs. 79, 87) for Bessel functions of the first kind and Neumann functions. This plot is shown in Fig. A1. The figure readily shows the change from oscillatory solutions to exponentially decaying solutions in the neighborhood of $\mu \doteq \xi$. In the oscillatory region, for the given order ($\doteq \sqrt{Ri_0}$ in our model), the function becomes infinitely oscillatory as the argument $\xi \to 0$.

Figure A1. Contour plot of the Bessel function $K_{i\mu}(\xi)$ in the (ξ, μ) plane. Negative regions are shaded. The format is selected for compatibility with Figures 79 and 87 of Jahnke, Emde, and Losch (1960).
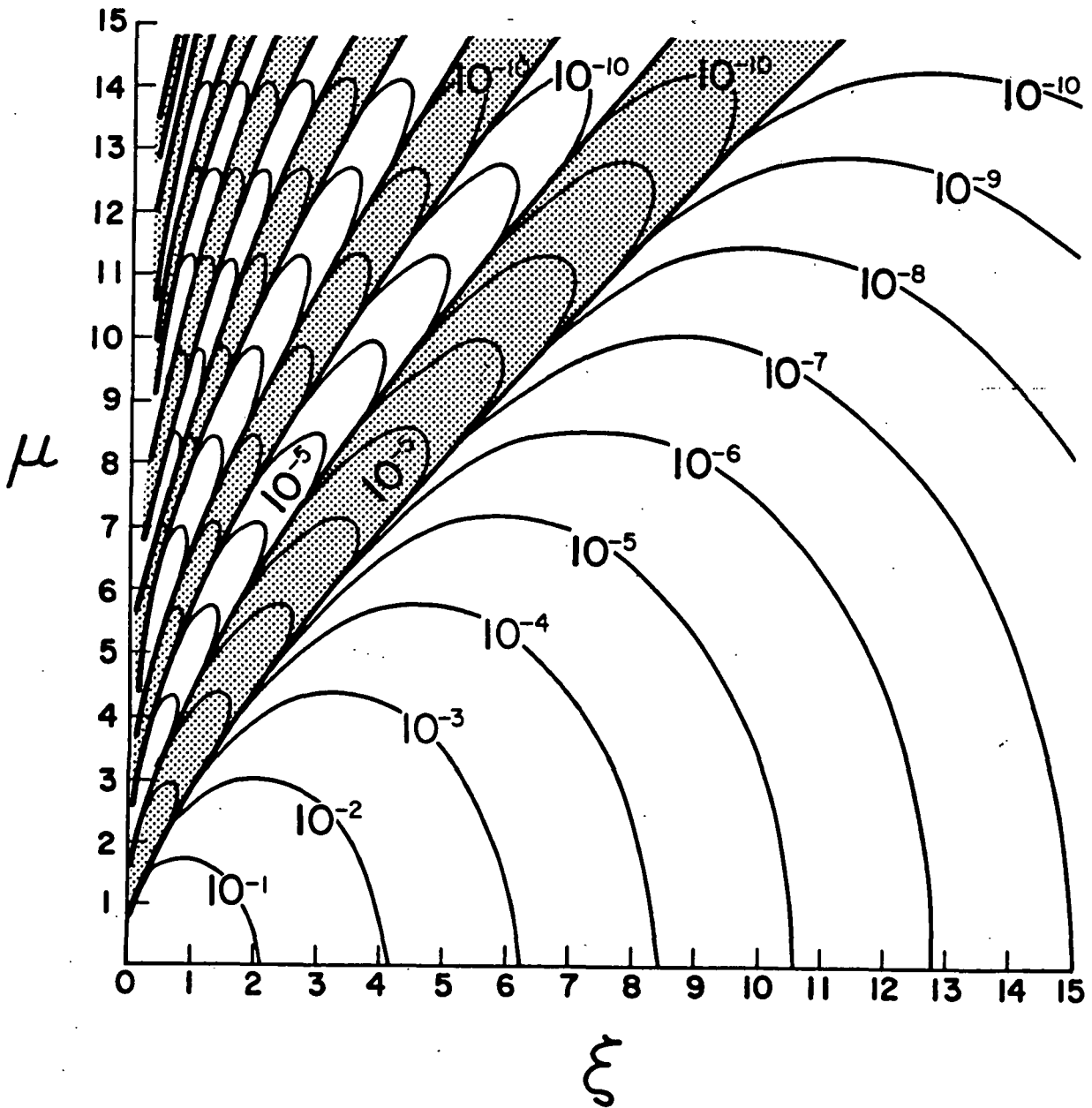
APPENDIX B

A transformation to (x,θ,t) coordinates requires the following identities:

$$\left(\frac{\partial}{\partial x}\right)_z = \left(\frac{\partial}{\partial x}\right)_\theta - \left(\frac{\partial z}{\partial x}\right)_\theta \left(\frac{\partial z}{\partial \theta}\right)^{-1} \left(\frac{\partial}{\partial \theta}\right)_z \tag{B1}$$

$$\left(\frac{\partial}{\partial z}\right)_x = \left(\frac{\partial z}{\partial \theta}\right)^{-1} \left(\frac{\partial}{\partial \theta}\right)_x \tag{B2}$$

$$\left(\frac{\partial \theta}{\partial z}\right)_x = \left(\frac{\partial z}{\partial \theta}\right)^{-1} \equiv \frac{N^2 \theta}{g} \tag{B3}$$

$$w = \frac{\partial z}{\partial t} + u \frac{\partial z}{\partial x} \qquad\qquad \frac{d\theta}{dt} = 0 \tag{B4}$$

All variables are total quantities and not perturbations.

For completeness we list the momentum equations in (x,θ)-coordinates although they will not be used here:

$$\frac{\partial u}{\partial t} + u \frac{\partial u}{\partial x} = -\theta \left[\frac{\partial \pi}{\partial x} - \frac{\partial z}{\partial x}\left(\frac{\partial z}{\partial \theta}\right)^{-1} \frac{\partial \pi}{\partial \theta} \right]$$

$$\left(\frac{\partial}{\partial t} + u \frac{\partial}{\partial x}\right)^2 z = -\theta \left(\frac{\partial z}{\partial \theta}\right)^{-1} \frac{\partial \pi}{\partial \theta} - g$$

where π is the barotropic pressure function

$$\pi = c_p (P/P_0)^{R/c_p}$$

The continuity equation in the non-hydrostatic system becomes time-dependent.

$$\frac{\partial}{\partial t}\left(\frac{\partial z}{\partial \theta}\right) + \frac{\partial}{\partial x}\left(u \frac{\partial z}{\partial \theta}\right) = 0 \tag{B5}$$

if the vorticity is defined as

$$\zeta = \frac{\partial w}{\partial x} - \frac{\partial u}{\partial z}$$

the vorticity equation

$$\frac{\partial \zeta}{\partial t} + \vec{v} \cdot \nabla \zeta = \frac{g}{\theta} \frac{\partial \theta}{\partial x}$$

becomes in the (x, θ)-system

$$\frac{\partial \zeta}{\partial t} + u \frac{\partial \zeta}{\partial x} = -\frac{g}{\theta}\left(\frac{\partial z}{\partial \theta}\right)^{-1} \frac{\partial z}{\partial x}$$